Stapp Car Crash Journal, Vol. 62 (November 2018), pp. 293-318

2018-22-0007

A Reanalysis of Experimental Brain Strain Data: Implication for Finite Element Head Model Validation

Zhou Zhou, Xiaogai Li, Svein Kleiven
Neuronic Engineering, KTH Royal Institute of Technology, Stockholm, Sweden

Chirag S. Shah
Humanetics Innovative Solutions, Inc., Farmington Hills, MI, USA

Warren N. Hardy
Virginia Tech-Wake Forest Center for Injury Biomechanics, Blacksburg, Virginia, USA

ABSTRACT – Relative motion between the brain and skull and brain deformation are biomechanics aspects associated with many types of traumatic brain injury (TBI). Thus far, there is only one experimental endeavor (Hardy et al., 2007) reported brain strain under loading conditions commensurate with levels that were capable of producing injury. Most of the existing finite element (FE) head models are validated against brain-skull relative motion and then used for TBI prediction based on strain metrics. However, the suitability of using a model validated against brain-skull relative motion for strain prediction remains to be determined. To partially address the deficiency of experimental brain deformation data, this study revisits the only existing dynamic experimental brain strain data and updates the original calculations, which reflect incremental strain changes. The brain strain is recomputed by imposing the measured motion of neutral density target (NDT) to the NDT triad model. The revised brain strain and the brain-skull relative motion data are then used to test the hypothesis that an FE head model validated against brain-skull relative motion does not guarantee its accuracy in terms of brain strain prediction. To this end, responses of brain strain and brain-skull relative motion of a previously developed FE head model (Kleiven, 2007) are compared with available experimental data. CORrelation and Analysis (CORA) and Normalized Integral Square Error (NISE) are employed to evaluate model validation performance for both brain strain and brain-skull relative motion. Correlation analyses (Pearson coefficient) are conducted between average cluster peak strain and average cluster peak brain-skull relative motion, and also between brain strain validation scores and brain-skull relative motion validation scores. The results show no significant correlations, neither between experimentally acquired peaks nor between computationally determined validation scores. These findings indicate that a head model validated against brain-skull relative motion may not be sufficient to assure its strain prediction accuracy. It is suggested that a FE head model with intended use for strain prediction should be validated against the experimental brain deformation data and not just the brain-skull relative motion.

KEYWORDS – Traumatic brain injury; finite element analysis; brain deformation; brain displacement; model validation;

INTRODUCTION

Traumatic brain injury (TBI) is complex injury associated with a wide spectrum of symptoms and detriment, ranging from mild levels, such as concussion that causes transient unconsciousness and nominal neurological impairment, to severe forms, such as diffuse axonal injury (DAI) that leads to prolonged coma accompanied by damage throughout the white matter of the brain (Gennarelli et al., 1982, Hardy, 2007, Kleiven, 2002). Although a complete understanding of the causation and effect relationship between mechanical input and associated brain injury remains to be developed, it has been reported that relative motion between the brain and skull and resultant brain deformation are primarily induced by rotational loading, which consequently trigger many types of brain trauma (Adams et al., 1981, Gennarelli et al., 1981, Hardy et al., 1994, Holbourn, 1943, Kleiven, 2002, Ommaya and Hirsch, 1971, Unterharnscheidt and Higgins, 1969). However, it is also understood that the transient intracranial

Address correspondence to Warren N. Hardy, Virginia Tech-Wake Forest Center for Injury Biomechanics, Blacksburg, Virginia, USA. Electronic mail: whardy@vt.edu

pressure elevation has negative effects on the brain (Chason et al., 1958, Gurdjian et al., 1961, Hardy, 2007, Kleiven, 2013, Masuzawa et al., 1976, Nahum et al., 1977, Nusholtz et al., 1984, Stalnaker et al., 1977, Trosseille et al., 1992, VandeVord et al., 2008, von Holst and Li, 2013) and is directly related to resultant linear acceleration measured at the center of gravity (c.g.) of the head (Hardy et al., 2007).

With advancement in imaging techniques, the study of brain-skull relative motion and brain deformation has progressed, although many details remain elusive. Substantial experimental efforts were made at Wayne State University (WSU), using bi-plane high-speed X-ray to track the motion of radiopaque targets implanted within the post-mortem human surrogate (PMHS) head-and-neck preparations subjected to various impact modes (Al-Bsharat et al., 1999, Hardy et al., 2001, Hardy et al., 2007). The radiopaque targets, or neutral density targets (NDTs), used in these tests, were made from tin granules encapsulated in polystyrene tubing. These experiments revealed that relative three-dimensional (3D) motion between the skull and the NDTs follow loop or figure-eight patterns with peak on the order of ± 5 mm. To further reduce the target's mass and minimize the volume of replaced brain tissue, Guettler et al. (2018) used tin granules without polystyrene capsules as targets to identify brain-skull relative motion under pure angular loading. In particular, Hardy et al. (2007) analyzed the motion of NDTs implanted in clusters, instead of in columns as in Al-Bsharat et al. (1999) and Hardy et al. (2001), to estimate strain in the PMHS brain. Deformation within the volume occupied by the implanted NDT clusters was quantified and described. The peak maximum principal and maximum shear strains were estimated to be on the order of 0.09. These studies are particularly important since they provide the brain deformation of human head specimens under impacts indicative of levels that could result in trauma.

Other imaging approaches have been used to quantify brain displacement and deformation. Margulies et al. (1990) and Meaney et al. (1995) adopted high-speed cinematography to film the deformation of the grid embedded within the gel-filled animal and human skull. The maximum shear strain was reported to be 0.05-0.22 under angular accelerations at levels associated with concussion or DAI. This grid approach was extended by Bayly et al. (2005) to in-vivo magnetic resonance imaging (MRI) sequences, in which tagged lines were inscribed to the imaging sequences to identify the brain deformation under voluntary motion. Due to the slow image acquisition rate, strain was estimated by evaluating different time points from manually repeated trials. Brain strain was estimated to be 0.02-0.05 for these low-speed events. This tagged MRI approach was subsequently implemented by Sabet et al. (2008) and Feng et al. (2010) under other voluntary loading scenarios, and improved by Knutsen et al. (2014). Another in-vivo brain motion characterization using MRI was reported by Ji et al. (2004) with special interest in the regions of brainstem and cerebellum. Recently, Alshareef et al. (2017) showed that sonomicrometry might have potential of measuring in-site whole brain motion under rotational loading. However, this technique implants the crystals in the brain as measuring targets, which are connected to external circuitry via wires. Tethering effect may be imposed on each crystal via the connecting wires. Since the signals are not acquired simultaneously as the crystals are activated sequentially, measurement error may arise because the leading edge or first few pulses of an ultrasonic burst are not registered by the sonomicrometer crystals. Given that the maximum throughput is fixed, the acquisition decreases as crystals are added. As summarized in Hardy (2002), this technique cannot be used in noisy environments.

In addition to the available experimental data, finite element (FE) models of the human head have become increasingly important to narrow the knowledge gaps between external loading and localized brain response and injury insight thereon. The biofidelity of such computational head models can be partially identified by validating the model's responses against available experimental data. Though claiming model validation, majority of the available FE head models have only compared their responses against experimental data under scanty scenarios, typically including the intracranial pressure data collected from the cortical and ventricular sites (Nahum et al., 1977, Trosseille et al., 1992) and/or brain-skull relative motion data measured from the regions where the NDTs occupied (Hardy et al., 2001, Hardy et al., 2007). Even when limited to the scanty cases outlined, none of the existing models have accurately reproduced brain-skull relative motion for all NDTs along all directions for all impacts (Drake et al., 2017, Giordano and Kleiven, 2016, Ho et al., 2017, Kleiven, 2006). It has been reported that a head model with reasonable brain pressure response does not necessarily guarantee an acceptable validity of the brain-skull relative displacement of the given model (Zhao et al., 2015, Zhou et al., 2018). This was supported by the numerical findings that the simulated brain displacement required unambiguous material representation while the model-computed pressure response exhibited almost no dependency on

the brain material properties (Bradshaw and Morfey, 2001, Kleiven and Hardy, 2002).

Strain-based metrics have been derived from a variety of computational studies to assess brain injury risk, such as maximum principal strain (MPS) (Kleiven, 2007), strain rate (Viano et al., 2005), the product of strain and strain rate (King et al., 2003), cumulative strain damage measure (CSDM) (Takhounts et al., 2008), axonal strain (Giordano and Kleiven, 2014, Zhao et al., 2017), etc. These strain based metrics are further used to establish kinematic based brain injury risk functions. For example, the Brain Injury Criteria (BrIC) of Takhounts et al. (2013) was derived using MPS and CSDM observed in two human head FE models: The SIMon (Simulated Injury Monitor) of DiMasi et al. (1995) and later Takhounts et al. (2008), and the GHBMC (Global Human Body Models Consortium) of Mao et al. (2013). Thus, direct evaluation of brain strain response of the computational model is important to ensure the confidence of using FE head models for TBI prediction based on strain metrics. The brain strain dataset of Hardy et al. (2007) has been used to evaluate the strain response of a handful of FE head models (Chafi, 2009, Chafi et al., 2009, Giordano and Kleiven, 2014, Giordano and Kleiven, 2016). However, Hardy et al. (2007) presented average strain of all cluster triads based on incremental displacement at each time-step for triads of NDT markers, which resulted in the incremental (or instantaneous) strains, though it was not explicitly described as incremental strain in the publication. This could lead to ambiguity in applicability of the previously published strain data being incremental or finite for FE head model validation.

In practice, it is commonly noted that FE head models validated against brain-skull relative motion are directly applied to infer potential brain injury risk based on strain metrics. A study by Zou et al. (2007) showed that the brain-skull relative motion of Hardy et al. (2001) could be separated into a rigid-body displacement component and a deformation component. Thus, the validity of implementing a model validated against only brain-skull relative motion for the brain strain prediction can be questionable.

In light of the importance of strain data for head model validation, the first objective of the current study is to calculate strains in Hardy et al. (2007) based on total displacement with respect to the initial NDT positions resulting in finite strain or just strain. The finite strain data are more relevant to evaluate the FE head models and subsequently for the brain injury prediction. A second objective is to use the revised brain strain data to test a hypothesis that a model validated against brain-skull relative motion cannot guarantee its accuracy in terms of brain strain prediction. This study provides important information for evaluating brain deformation of FE head models.

METHODS

Experimental data

Thirty-five impacts were conducted by Hardy et al. (2007) on eight inverted and perfused head and neck complexes of PMHS. The specimens were brought to speed using a pneumatic piston device, and then impacted a stationary rigid surface. The generalized 3D kinematics of the head was measured using a nine-accelerometer tetrahedral package. A high-speed, biplane X-ray system was used to track the motion of the radiopaque NDTs implanted within the cadaveric brain. The NDT coordinates and motion were obtained with respect to an anatomical coordinate system with the c.g. of the head being the origin. Through coordinate system transformation, the rigid-body motion of the skull was eliminated from each of the NDT motion data, leaving the brain-skull relative displacements to facilitate the estimation of local strain parameters within the brain. For each cadaver brain, two NDT clusters were implanted with seven targets in each cluster. The NDT clusters were implanted in a variety of configurations depending upon the testing conditions (Figure 1 (a)). For each impact, the NDT clusters and locations were numbered. As demonstrated by C380-T2 in Figure 1(b), NDTs 1-7 comprised cluster 1 (C1) in the contrecoup side with NDT 4 as the center target, while NDTs 8-14 comprised cluster 2 (C2) in the coup side with NDT 11 as the center target. The NDT numbering convention was in general consistent, but varied slightly for a few clusters. For each impact, the available NDT tracking intervals, starting positions and peak excursions were tabulated. A representative case is reproduced in Table 1.

LS-DYNA (Livermore Software Technology Corporation, LSTC) was used to calculate strain parameters for each cluster using multiple triads of targets as described in Hardy et al. (2007). For each NDT cluster, representative FE nodes were generated based on the NDT starting position. Each node was connected to its neighboring nodes to form a 3-node FE shell element referred hereafter as triad. Of all the available clusters, the number of triads was variable depending on the availability of tracked data for the targets that formed a given triad. When the center target was available, up to twelve triads were formed as shown on the left of Figure 1 (c). When the center

target was missing, up to eight triads were formed on the surface of the cluster as shown on the right of Figure 1 (c). Maximum principal and shear strains were obtained from the simulation by imposing the tracked NDT motion in experiments relative to the skull on the NDT triad model. Since 3D displacements were prescribed to all FE nodes of the triad as described above, resultant strain responses are independent from the modelling choices, such as element formulation, material properties, etc. The results from all available triads were averaged for each NDT cluster (referred as average cluster strain). Average strain rate was acquired by taking time derivative of the average strain responses. However, as mentioned, strain was calculated based on incremental displacements for triads of NDT markers.

(a)

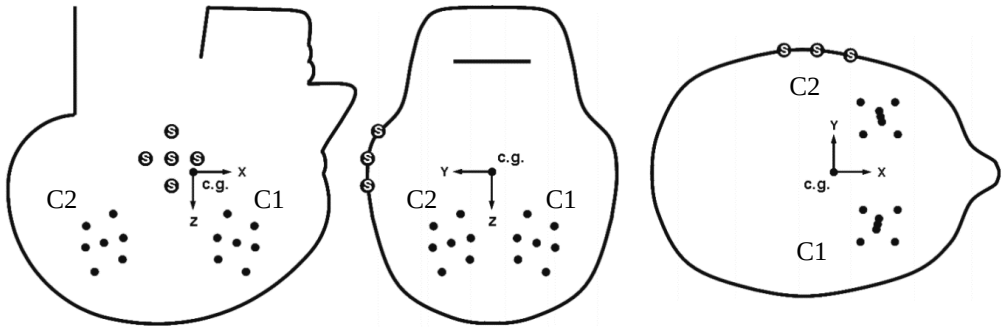

(b)

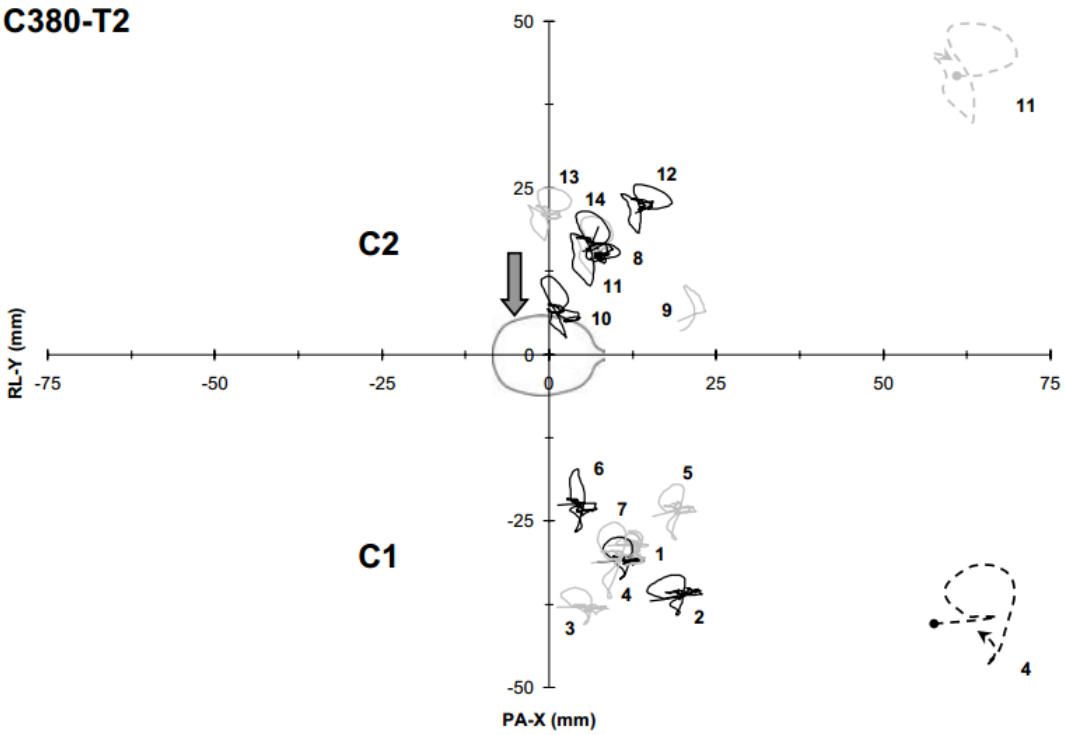

(c)

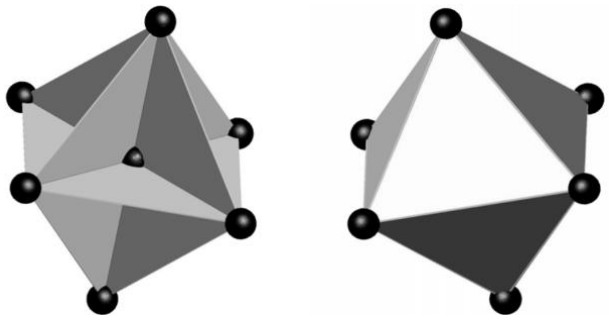

Figure 1. (a) The general NDT cluster implanting schemes for tests involving impact in the median plane (left), coronal plane (middle), and horizontal plane (right). For most median impacts, C1 was placed in the frontal lobe and C2 was placed in the parietal lobe, both being on the right side. For the coronal or horizontal impacts, C1 was placed in the right hemisphere, and C2 was placed in the left hemisphere, both being in the parietofrontal regions. The large markers designated "S" were attached to the skull, defining the body-fixed basis. (b) Brain-skull relative motion patterns for C1 and C2 for test C380-T2 of a horizontal impact. (c) The NDT triad model used for calculating strain responses. This figure is adapted from Hardy et al. (2007) and reprinted with permission of the Stapp Association.

Table 1. NDT tracking intervals, starting positions, and peak excursions for test C380-T2, adapted from Hardy et al. (2007) and reprinted with permission of the Stapp Association.

Cluster		C2							C1						
NDT #		14	13	12	11	10	9	8	7	6	5	4	3	2	1
Interval (ms)	Start	0	0	0	0	0	0	0	0	0	0	0	0	0	0
	Stop	252	247	252	252	242	49	252	222	206	231	225	219	225	228
Start position (mm)	X	5.07	-1.19	12.92	5.40	-0.19	19.29	6.15	6.28	1.23	15.56	7.29	1.19	15.13	8.79
	Y	15.53	20.98	21.27	16.01	6.45	5.04	14.50	-31.33	-22.57	-24.33	-31.16	-37.93	-37.08	-28.70
	Z	53.68	47.58	46.83	47.11	45.50	42.48	37.42	52.36	44.67	45.38	42.45	41.76	43.61	34.46
Peak excursion (mm)	X	4.52	4.49	5.43	4.13	4.88	4.12	4.47	8.01	5.92	6.39	6.92	7.56	7.75	6.07
		-1.84	-1.94	-2.20	-1.65	-1.04	0.00	-0.60	0.00	0.00	0.00	0.00	0.00	-0.46	0.00
	Y	5.96	4.01	4.24	4.62	5.27	5.32	2.19	6.14	5.36	4.83	3.72	2.91	3.98	2.19
		-5.25	-3.91	-3.11	-4.05	-3.92	-1.49	-0.82	-5.37	-4.03	-3.49	-2.53	-2.66	-2.02	-1.78
	Z	2.79	3.24	3.41	2.98	2.67	2.66	2.94	5.44	5.21	4.55	5.43	6.09	5.15	5.37
		-0.87	-1.74	-1.96	-0.68	-0.69	0.00	-0.26	0.00	0.00	0.00	0.00	-1.01	-0.76	0.00

Cluster Strain recalculation

The strain responses over all the clusters are recalculated following the approach described by Hardy et al. (2007) (referred as NDT triad approach), which uses total displacement with respect to the initial NDT positions. The following criteria are developed to assess the eligibility of the NDT clusters for strain recalculation:

1) Criterion of kinematics availability, namely the availability of the experimental kinematics.

To ensure the brain deformation data are applicable to FE head model strain validation, robust kinematics response data are needed. Tests for which the nine-accelerometer array was damaged or decoupled are excluded.

2) Criterion of measurement accuracy, namely the accuracy of the NDT motion measurement.

NDT motion measurement accuracy is evaluated based on the relevant description in Hardy et al. (2007). Traces of the NDTs that contain potential error sources are removed from strain calculation. Those NDTs whose motion patterns did not exhibit the trends toward their initial positions are also discarded.

3) Criterion of NDT data sufficiency, namely the availability of NDT start positions to establish the triad model and the sufficiency of the remaining trajectories to prescribe the boundaries of the NDT triad model.

Due to the interference imposed by the experimental hardware, not all targets for all tests could be tracked. Targets whose initial positions at the time of contact were not available should be excluded also. After discarding those NDTs lacking initial position data, only those clusters for which either all associated seven targets are available (corresponding to the NDT triad model on the left of Figure 1(c)), or only the center target is missing (corresponding to the NDT triad model on the left of Figure 1(c)), are retained for strain calculation.

The original strain calculations involved extending the data as far in time as possible by fewer number of triads that had reliable NDT motion data. This means that the number of targets, and therefore triads, contributing to the average calculation varied for some clusters. The strain interval, or calculation duration, for a given cluster should be that of the shortest motion tracking interval/duration of any of the six or seven NDTs comprising the cluster. This is the minimum NDT motion interval for a cluster. A protocol is established to determine the cluster strain recalculation time interval:

1) For those clusters with a minimal NDT motion duration over 120 ms, the strain interval is set as 120 ms, same as in Hardy et al. (2007).

2) For those clusters with a minimal NDT motion duration less than 120 ms, the strain interval is set as the same value of the minimal NDT motion duration.

For the revised strain calculations, principal strain and shear strain (Green-Lagrangian strain) are derived from each triad element and all triads are averaged within the cluster, i.e. average cluster strain. Strain rate is calculated by taking time derivative of

the averaged strain responses. The product of strain and strain rate is computed by taking the product of the instantaneous strain and strain rate.

The peak average strain is calculated for each cluster. Correspondingly, the peak average brain-skull relative motion for each cluster (referred as average cluster brain-skull relative motion) is determined as the peak of the averaged motion responses of associated 6 or 7 NDTs within the cluster strain interval. The Pearson correlation coefficient is determined to assess the correlation between the peak average cluster strain and the peak average brain-skull relative motion. Correlation is considered significant for $p<0.01$.

Experimental simulation

The revised brain strain data, together with the brain-skull relative motion data, are used to test the hypothesis that a model validated against brain-skull relative motion cannot guarantee its accuracy in terms of brain strain prediction. The KTH (Kungliga Tekniska Högskolan) head model, developed by Kleiven (2007), is selected for this purpose. This model includes the scalp, the skull, the brain, the meninges, the cerebrospinal fluid (CSF), the ventricles, the superior sagittal sinus, the transverse sinus, a simplified neck with the extension of the spinal cord, and 11 pairs of parasagittal bridging veins (Figure 2). The model is described with greater detail in Kleiven (2007).

Both brain strain and brain-skull relative motion validations are performed using the KTH head model. In Hardy et al. (2007), the durations of the NDT traces were much longer than those of the acceleration pulses (typically, acceleration pulses of 10-15 ms compared to NDT traces of 120 ms). The relative brain-skull motion described by the NDTs was shown to correspond to the angular speed characteristics of the head, which were typified by long duration. To capture the typical looping pattern of the local brain motions, simulations of at least 40-ms long are required (Giordano and Kleiven, 2016). Thus, clusters with strain intervals over 40 ms are selected for analysis. The measured kinematics are used to drive the model at the node that represents the c.g. of the corresponding cadaver. This node is rigidly coupled to the skull. To approximate the specimen anthropometry, the KTH head model is scaled to match the reported cadaver head dimensions. The node nearest to the start position of an experimental NDT target is taken as the marker location in the model. Motions of the identified nodes with respect to the skull along three anatomical coordinate directions are obtained from the whole head model simulation. Following the NDT triad approach described by Hardy et al. (2007), the initial positions of the identified nodes and the nodal motion responses predicted in the model are used to calculate the strain responses, specifically first principal Green-Lagrangian strain and shear Green-Lagrangian strain, of the brain model.

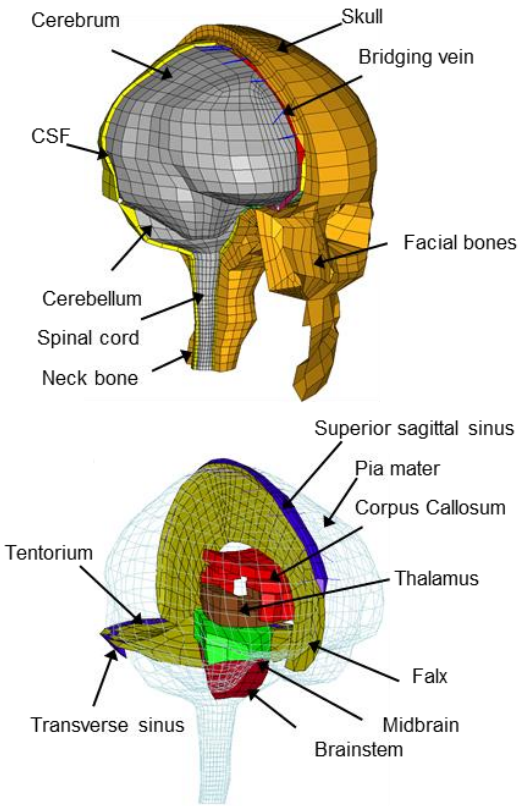

Figure 2. Finite element model of the human head.

Validation of the model performance is evaluated using two approaches: CORrelation and Analysis (CORA) (Version 3.4) and Normalized Integral Square Error (NISE). The technical details are available in Gehre et al. (2009) for CORA and in Donnelly et al. (1983) for NISE. Briefly, CORA scores the similarity of experimental data and model responses by a combination of cross correlation rating in terms of shape (V), size (G), and phase (P), and corridor rating (C1). NISE evaluates the agreement between the experimental measurement and model prediction in three aspects, including phase (N-phase), amplitude (N-amp), and shape (N-shape). For CORA, the scores range from 0 to 1, with 1 indicating a perfect match. For NISE, the scores range from 0 to 100, with 100 indicating a perfect match. The validation ratings regarding brain-skull relative motion and brain strain are computed for each NDT cluster using CORA and NISE. For the

brain-skull relative motion, the validation rating is calculated by simultaneously accounting for the motion of seven affiliated NDTs along three anatomical axes. For the brain strain, the validation rating is obtained by averaging the scores of the principal strain and shear strain. The evaluation intervals are consistently set to 40 ms. For the CORA, the global setting recommended by Giordano and Kleiven (2016) is employed with a modification that both the corridor rating and cross correlation rating are performed. In Giordano and Kleiven (2016), only the cross correlation rating was performed.

The Pearson correlation coefficient is determined to assess correlation between the brain strain validation scores and brain-skull relative motion validation scores. Correlation analyses are performed on each evaluating term and the resultant average values for both CORA and NISE. Correlation is considered significant for $p<0.01$.

RESULTS

Revised strain results

70 NDT clusters from 35 impacts are evaluated in terms of their eligibility for strain recalculation following the criteria of kinematics availability, measurement accuracy, and NDT data sufficiency (Table 2).

As described in Hardy et al. (2007), no kinematics data were measured for C288-T4 since the nine-accelerometer package was damaged during the earlier test. For C472, the nine accelerometer array decoupled from its mount. Kinematics data for the four experimental impacts delivered to the C472 could not be obtained. Therefore, a total of 10 NDT clusters, out of the foregoing 5 impacts, were excluded due to unavailability of experimental kinematics.

Hardy et al. (2007) purposely placed the NDTs on the cortical surface in C408 to illuminate the nature of the brain-skull interface. Whereas, less confidence was expressed by Hardy et al. (2007) regarding the accuracy of measured NDT motions given the substantial differences between the motion responses on the cortical and subcortical region, suggesting the targets had escaped the confines of the cortex for this specimen. Therefore, 10 NDT clusters from the five impacts involving C408 were eliminated due to the suspected measurement inaccuracy. For the six impacts delivered to C380, motion of the NDT 9 affiliating to C2 failed to exhibit a motion trend toward its starting position. Measurement inaccuracy is suspected for this specific NDT also. Thus, 6 NDT clusters from these six impacts are discarded.

The NDTs that could not be tracked were naturally excluded. NDTs for which there were no data at contact were discarded also. Of the remaining clusters, only those containing all seven NDTs, or those missing only the center NDT, were retained for triad formation and analysis. Applying the NDT trace sufficiency criterion, 29 NDT clusters were eliminated.

Consequently, 15 NDT clusters from 14 impacts meet the criteria and are suitable for calculating the strain parameters using the NDT triad approach. Out of the 15 recalculated clusters, the NDT numbering convention is consistent with the exception of C288-T3 C1 in which NDT 6 and NDT 7 were interchanged, and C064-T1 C1 in which NDT 4 and NDT 6 were interchanged. All of the 15 recalculated clusters followed the model on the left of Figure 1 (c).

The cluster strain calculation time durations are re-evaluated as well. For example, the interval for C380-T2 C1 is set to 120 ms, given that the minimum NDT motion duration was 206 ms (NDT 6), which exceeds 120 ms. The interval for C380-T1 C1 is set to 64 ms, which is established by the motion tracking duration of NDT 2 (64 ms). The duration for all revised cluster strains are summarized in Table 3.

All the revised principal strain and shear strain data are plotted in Figure 3, along with the original data from Hardy et al. (2007) to illustrate the difference between the revised values and the original incremental data. Table 3 catalogs the peak strain of the original dataset and the revised values. Note that for the original data, only the peaks of the 6 clusters with a valid cluster strain interval are listed. For the 6 clusters with the same strain intervals between the origin and revision, the average peak differences are -201.9% for principal strain and -247.2% for shear strain. Further, the peak average strain rate differences are -49.7% for principal strain and -40.9% for shear strain, while peak average strain and strain rate product differences are 269.2% for principal strain, and 395.7% for shear strain.

When looking into the 15 recalculated cases alone, the largest peak principal strain is 0.094 in C288-T3 C2 and C380-T6 C1, while largest peak shear strain is 0.091 in C380-T4 C1. The greatest peak principal strain rate is 14.8 /s in C393-T2 C1, while the greatest peak shear strain rate is 16.8 /s in C288-T3 C1. The greatest peak strain and strain rate product is

0.715 for principal strain and 0.802 for shear strain in C288-T3 C1.

The peak average cluster strain and peak average cluster brain-skull relative motion from all 15 recalculated clusters are plotted in Figure 4. No significant correlations are observed between the experimentally measured relative motion peaks and strain peaks, neither for principal strain (correlation coefficient: -0.039, p=0.889) nor for shear strain (correlation coefficient: -0.035, p=0.900).

Considering the scarcity of coronal and horizontal impacts in Hardy et al. (2007) and the consistency of the suspected NDT traces for the six impacts delivered to C380, an exceptional configuration is developed to derive the strain in C2 based on the six remaining NDTs with reliable traces. Results are presented in Appendix A in detail and can be optionally used by the future modeler.

Table 2. Selection of the NDT cluster in each experimental case for strain recalculation. The symbols yes (Y)/no (N) are used to indicate pass/fail of a certain criterion.

Specimen and test		Impact plan	Kinematics availability	Measurement accuracy		NDT data sufficiency		Selected for revised strain calculation	
				C1	C2	C1	C2	C1	C2
C288	T1	Sagittal	Y	Y	Y	N	N	N	N
	T2		Y	Y	Y	N	N	N	N
	T3		Y	Y	Y	Y	Y	***Y***	***Y***
	T4		N	Y	Y	Y	Y	N	N
C241	T1	Sagittal	Y	Y	Y	N	N	N	N
	T2		Y	Y	Y	N	N	N	N
	T3		Y	Y	Y	N	N	N	N
	T4		Y	Y	Y	N	N	N	N
	T5		Y	Y	Y	N	Y	N	***Y***
	T6		Y	Y	Y	N	Y	N	***Y***
C015	T1	Sagittal	Y	Y	Y	N	N	N	N
	T2		Y	Y	Y	N	N	N	N
C064	T1	Sagittal	Y	Y	Y	Y	N	***Y***	N
	T2		Y	Y	Y	N	N	N	N
	T3		Y	Y	Y	N	N	N	N
	T4		Y	Y	Y	N	N	N	N
C380	T1	Coronal	Y	Y	N	Y	N	***Y***	N
	T2	Horizontal	Y	Y	N	Y	N	***Y***	N
	T3	Coronal	Y	Y	N	Y	N	***Y***	N
	T4		Y	Y	N	Y	N	***Y***	N
	T5	Horizontal	Y	Y	N	Y	N	***Y***	N
	T6	Coronal	Y	Y	N	Y	N	***Y***	N
C393	T1	Coronal	Y	Y	Y	Y	N	***Y***	N
	T2		Y	Y	Y	Y	N	***Y***	N
	T3		Y	Y	Y	Y	N	***Y***	N
	T4		Y	Y	Y	Y	N	***Y***	N
C408	T1	Sagittal	Y	N	N	N	N	N	N
	T2		Y	N	N	N	N	N	N
	T3		Y	N	N	N	N	N	N
	T4		Y	N	N	N	N	N	N
	T5		Y	N	N	Y	N	N	N
C472	T1	Sagittal	N	Y	Y	Y	Y	N	N
	T2		N	Y	Y	Y	Y	N	N
	T3		N	Y	Y	Y	Y	N	N
	T4		N	Y	Y	Y	Y	N	N

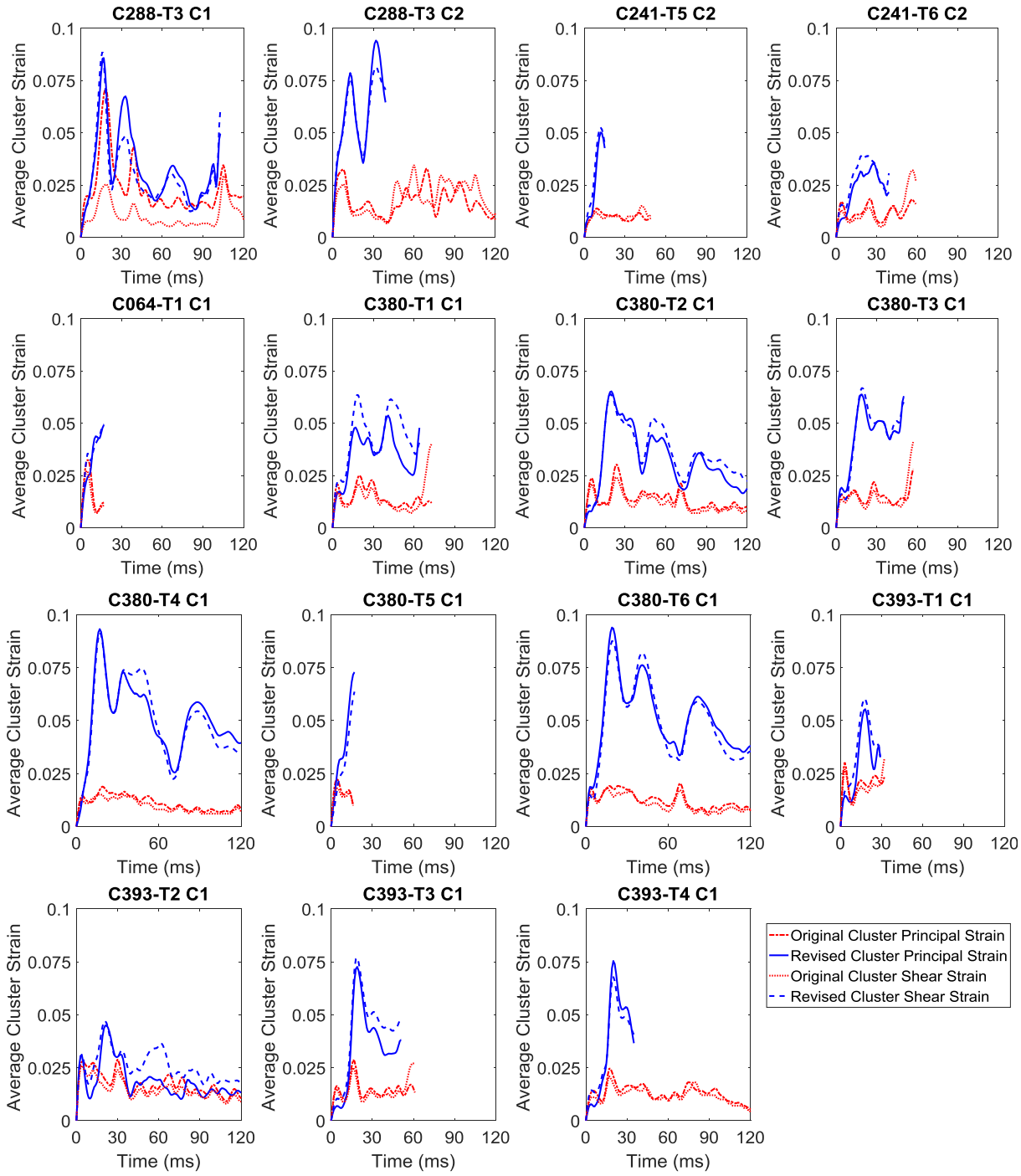

Figure 3. Comparison of strain response of 15 NDT clusters between the original and recalculated results. Average cluster strain is referred as average maximum strain in Hardy et al. (2007).

Table 3. Cluster strain interval and peak values of the strain responses of the original and recalculated results

NDT cluster	Duration (ms)		Strain				Strain rate (/s)				Strain*Strain rate (/s)			
			Principal		Shear		Principal		Shear		Principal		Shear	
	Original	Revised	Original	Revised	Original	Revised	Original	Revised	Original	Revised	Original	Revised	Original	Revised
C288-T3 C1	120	103		0.086		0.089		13.2		16.8		0.715		0.802
C288-T3 C2	120	39		0.094		0.081		13.3		14.0		0.593		0.400
C241-T5 C2	49	15		0.050		0.053		8.8		7.9		0.292		0.296
C241-T6 C2	59	40		0.035		0.039		3.5		6.4		0.064		0.160
C064-T1 C1	17	17	0.033	0.049	0.027	0.050	36.7	8.0	28.7	8.9	0.248	0.224	0.173	0.197
C380-T1 C1	73	64		0.054		0.064		7.6		9.4		0.313		0.274
C380-T2 C1	120	120	0.030	0.065	0.024	0.064	5.1	8.0	4.9	7.9	0.103	0.354	0.068	0.335
C380-T3 C1	57	50		0.064		0.067		8.2		6.8		0.431		0.306
C380-T4 C1	120	120	0.019	0.093	0.015	0.091	17.3	10.4	17.1	10.5	0.059	0.688	0.051	0.679
C380-T5 C1	17	17	0.022	0.073	0.018	0.064	40.8	6.0	27.6	10.6	0.217	0.366	0.120	0.529
C380-T6 C1	120	120	0.020	0.094	0.018	0.088	33.4	8.2	26.5	8.23	0.145	0.566	0.100	0.527
C393-T1 C1	47	30		0.055		0.060		7.7		8.31		0.284		0.288
C393-T2 C1	120	120	0.029	0.045	0.026	0.047	56.1	14.8	44.4	13.9	0.391	0.221	0.292	0.200
C393-T3 C1	61	51		0.073		0.077		12.8		12.7		0.642		0.705
C393-T4 C1	129	35		0.075		0.068		13.8		12.4		0.706		0.580

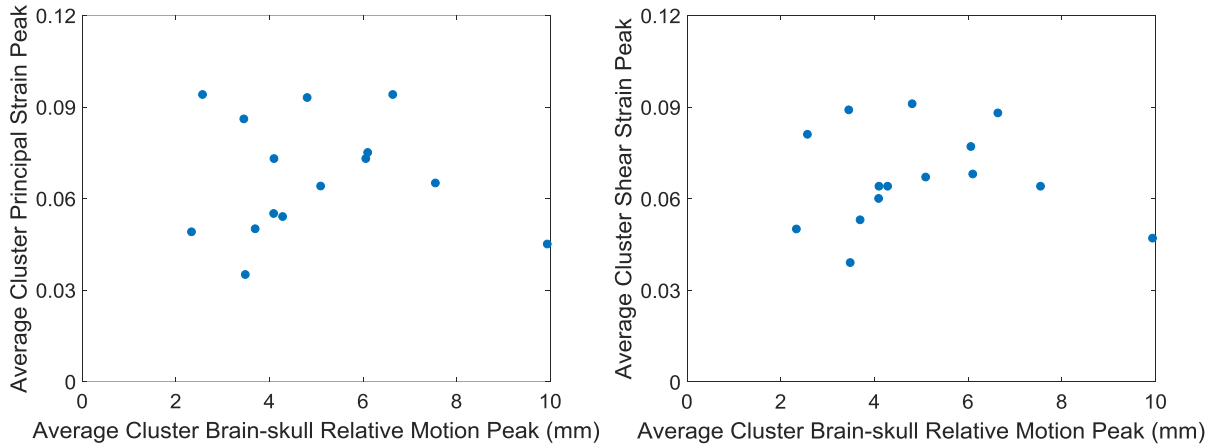

Figure 4. Scatter plot showing average peak cluster brain-skull relative motion and peak average cluster strain (left: principal strain; right: shear strain).

Experimental simulation results

Brain-skull relative motion and brain strain responses of a total of 8 NDT clusters with strain intervals over 40 ms from 8 impacts are simulated, including C288-T3 C1, C380-T1 C1, C380-T2 C1, C380-T3 C1, C380-T4 C1, C380-T6 C1, C393-T2 C1, and C393-T3 C1. Model-predicted average cluster principal strain and average cluster shear strain results are plotted in Figure 5. Corresponding figures for the brain-skull relative motion validation results are provided in Appendix B.

Model validation scores for each evaluation term and the resulting average values are provided in Figure 6 for CORA and in Figure 7 for NISE. By averaging the ratings of the 8 NDT clusters, four overall validation scores are obtained with values of 0.57 for CORA and 75.22 for NISE for brain strain, and 0.40 for CORA and 92.27 for NISE for brain-skull relative motion. No significant correlations are observed between the brain strain validation score and brain-skull relative motion validation score for any evaluation terms ($p < 0.01$) (Table 4).

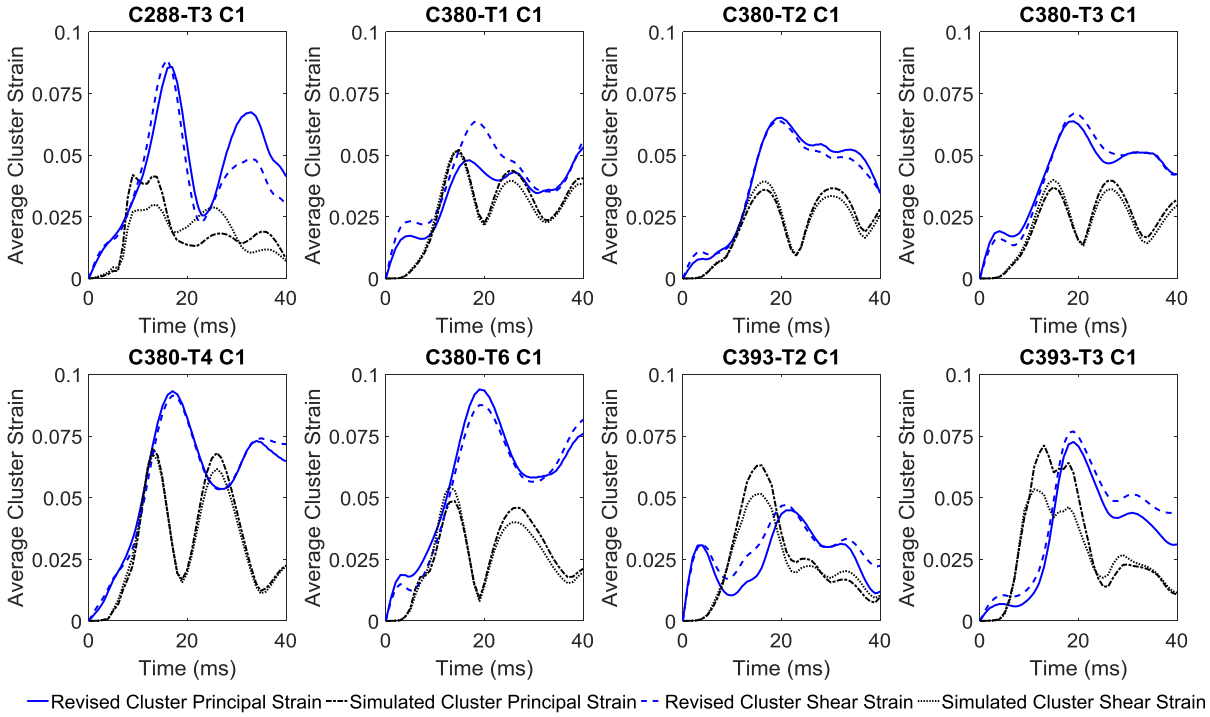

Figure 5. Comparison between recalculated experimental strain data and simulated brain strain responses.

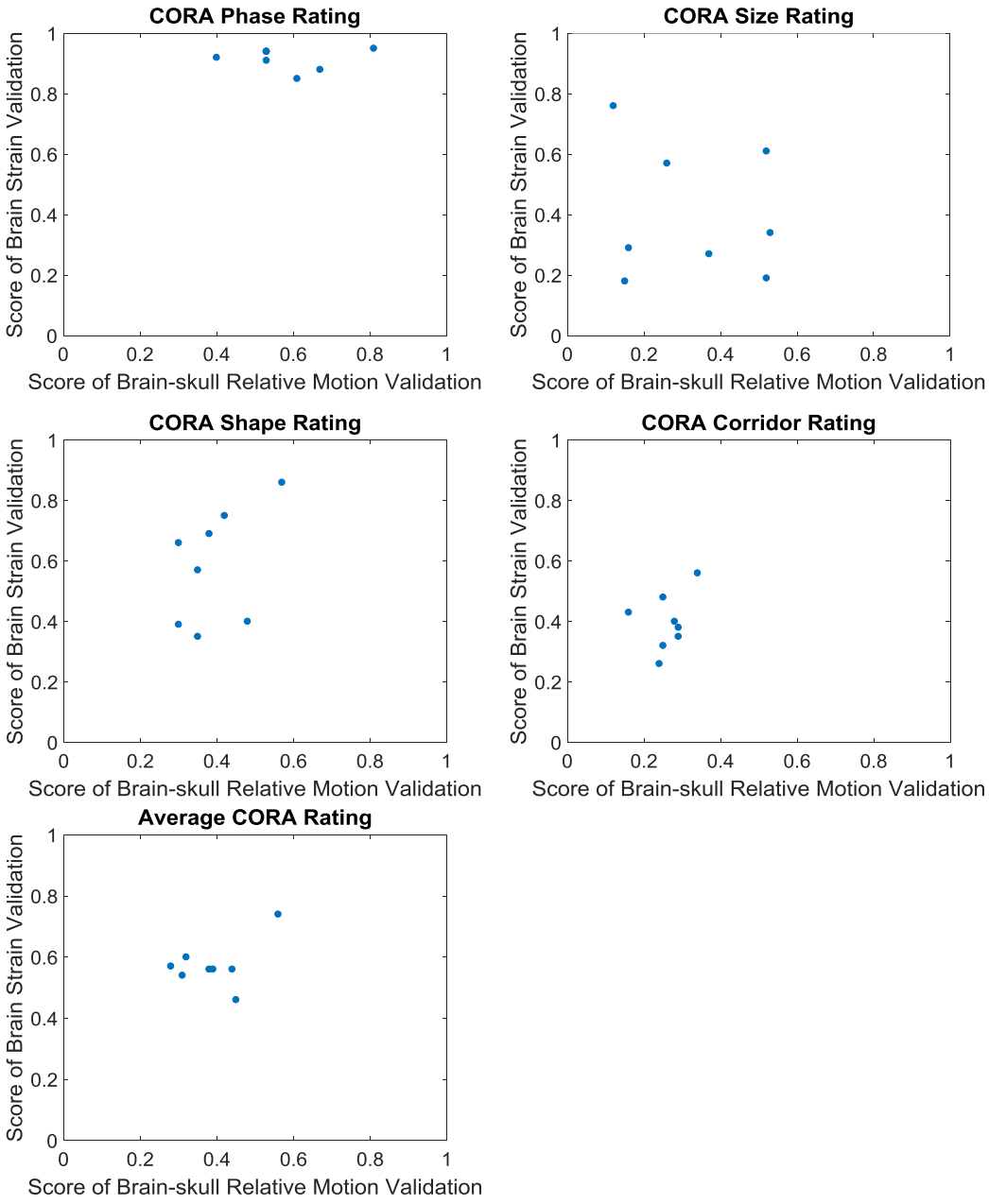

Figure 6. Scatter plot showing CORA scores for brain strain validation and brain-skull relative motion validation using 8 NDT clusters.

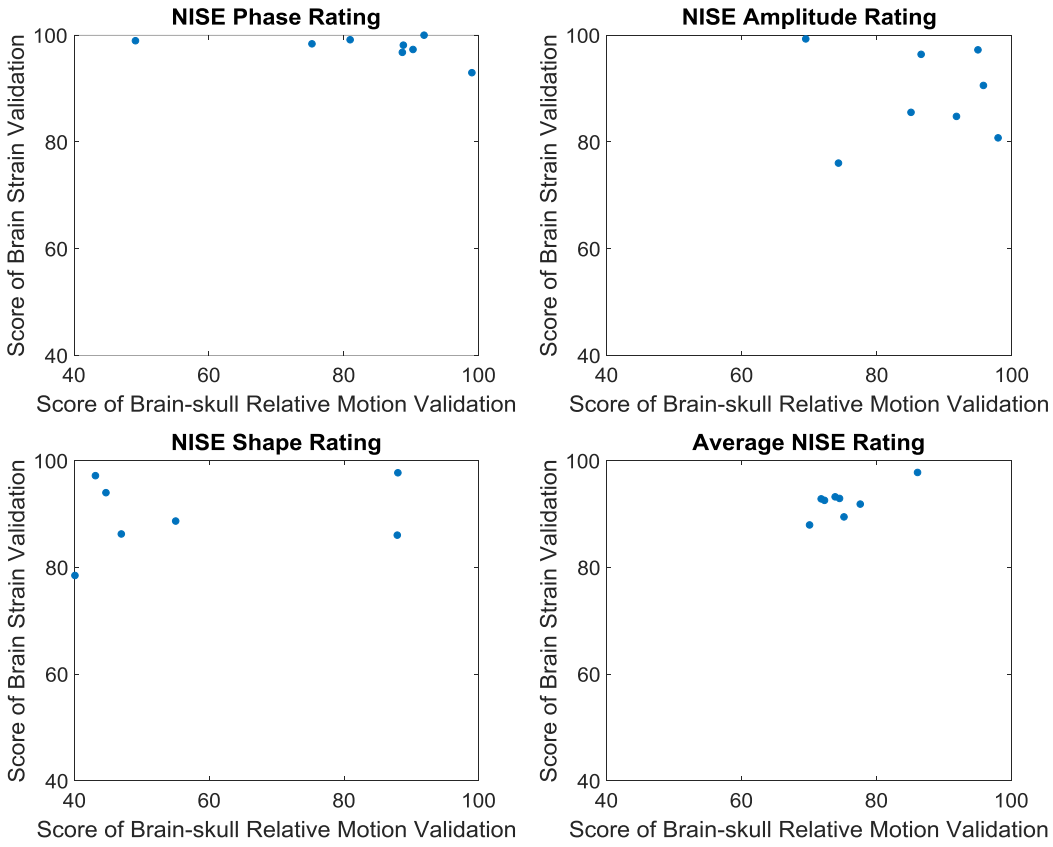

Figure 7. Scatter plot showing NISE scores for brain strain validation and brain-skull relative motion validation using 8 NDT clusters.

Table 4. Pearson correlation coefficients and associated probabilities between brain strain validation scores and brain-skull relative motion validation scores.

CORA			NISE		
Term	Correlation coefficient	p value	Term	Correlation coefficient	p value
Phase	-0.047	0.912	Phase	-0.476	0.233
Size	-0.171	0.685	Amplitude	-0.071	0.868
Shape	0.470	0.240	Shape	0.225	0.592
Corridor	0.307	0.460	--	--	--
Average	0.442	0.273	Average	0.742	0.068

DISCUSSION

This study provides revised calculations of strain parameters based upon NDT motion originally presented in Hardy et al. (2007). The revised brain strain data together with the brain-skull relative motion data are then used to evaluate the KTH head model. CORA and NISE are employed to validate the model validation performance for both brain strain and brain-skull relative motion. Correlation analyses are conducted to compare experimentally measured peak average cluster strain and peak average cluster brain-skull relative motion, and to compare brain strain validation scores and brain-skull relative motion validation scores. No significant correlations are noted, neither for experimentally acquired peaks nor computationally determined validation scores. The lack of correlations indicates that a brain model validated with brain-skull relative motion could not guarantee its strain prediction accuracy, reinforcing the need that a model to be used for strain prediction should evaluate its brain deformation against the experimental brain strain data.

Strain response considerations

A concise comparison of strain peaks in both the original and revised datasets to earlier studies is

provided in Table 5. The revised peak average strain are generally consistent with the quantitative studies of Margulies et al. (1990) and Meaney et al. (1995), in which the gel brain simulant used in animal and human skull models deformed when subjected to angular acceleration levels similar to those used by Hardy et al. (2007). The revised strain values are about two to three times larger in magnitude than the peak strain measured from volunteer testing, whose loading conditions were far from injury levels (Bayly et al., 2005, Feng et al., 2010, Sabet et al., 2008).

The first attempt to use the strain dataset in Hardy et al. (2007) for the validation purpose is reported by Chafi et al. (2009) and Chafi (2009), in which the strain response of the University College Dublin Brain Trauma Model (UCDBTM) (Horgan and Gilchrist, 2003) were evaluated. It was found that the brain strain estimated by the UCDBTM were consistently larger than the original incremental strain calculations under a range of brain and CSF constitutive representations, and shear moduli spanning an order of magnitude. Mayberry (2008) used an analytical brain injury model (Zou et al., 2007) to reconstruct two coronal impacts from Hardy et al. (2007). The analytical strain results were nearly double in magnitude than those in Hardy et al. (2007). The strain estimated by the UCDBTM and the analytical model agree better with the revised strain data presented herein. In contrast, Giordano and Kleiven (2014) and Giordano and Kleiven (2016) validated the brain strain responses of four popular FE head models (Giordano et al., 2014, Iwamoto and Nakahira, 2015, Kleiven, 2007, Mao et al., 2013), arriving at strain magnitudes comparable to the original incremental strain calculations. It is important to note that an inspection has disclosed issues in Giordano and Kleiven (2014) and Giordano and Kleiven (2016) regarding deriving strain from the whole head simulations. A revised study is planned for the future.

Table 5. Comparison of peak brain strain from available studies.

Approach	Study	Acceleration	Peak strain
Physical model	Margulies et al. (1990)	Rotation: 3700-69600 rad/s^2	Shear strain: 0.07-0.22
	Meaney et al. (1995)	Rotation: 5000-200000 rad/s^2	Shear strain: 0.05-0.17
Volunteer test	Bayly et al. (2005)	Translation: 2-3 g	Principal strain: 0.02-0.05
	Sabet et al. (2008)	Rotation: 250-300 rad/s^2	Principal strain: 0.06
	Feng et al. (2010)	Translation: 1.5 g Rotation: 120-140 rad/s^2	Principal strain: 0.05-0.07
PMHS test	Hardy et al. (2007)	Translation: 38-291 g Rotation: 2370-24206 rad/s^2	Principal strain: 0.088 Shear strain: 0.089
	Current study		Principal strain: 0.094 Shear strain: 0.091

Relationship between brain and skull kinematics

Figure 8 (a) illustrates the trends for selected kinematics responses for test C288-T3, which was an occipital blow resulting in sagittal rotation. The relationships between linear head acceleration in the X direction, angular speed of the head about the Y axis, brain motion in the X direction, and averaged principal strain for C1 are compared. Following the approach outlined by Hardy et al. (2007), the ordinate units are arbitrary for the purpose of comparing trends. Initially, the head experiences slightly rearward rotation, and then near 5 ms begins the dominant motion, which was forward rotation. The linear acceleration in the direction of impact peaks near 5 ms, and ends near 8 ms. The relative brain displacement and strain response continuously increase by this time. During the interval from 5 ms to 13 ms, the angular speed of forward head rotation increases with peaking near 7 ms, and subsequently decreases while maintaining positive magnitude, and then increases again. The relative displacement crests as the angular speed reaches its second peak near 13 ms, which is also close to the principal strain peak time (near 15 ms). Thereafter, the relative displacement decreases following the decreasing trend of the angular speed. When the displacement crosses zero near 23 ms implying that the brain returns to its neutral position, a local minimum in the

strain response occurs. As the angular speed continuously decreases, the relative displacement deviates from neutral and becomes positive. The strain exhibits a local maximum as the relative displacement peaks positively near 32 ms. At the time angular speed changes direction near 54 ms, the brain again returns to neutral accompanied by a local minimum in the strain response. As the angular speed becomes more negative, the brain once again moves away its neutral configuration. The relative displacement reaches its peak positively at 82 ms and subsequently decreases to zero at 100 ms.

Figure 8 (b) illustrates the trends for selected kinematics responses for test C380-T1, which was a temporal blow resulting in coronal rotation. The relationships between linear head acceleration in the Y direction, angular speed of the head about the X axis, brain motion in the Y direction, and averaged principal strain for C1 are compared. The ordinate units are arbitrary. The linear acceleration pulse in the direction of impact peaks near 5 ms, which approximately coincides with the time of the principal strain exhibiting a local maximum. The angular speed of the head increases to its maximum near 20 ms, which is followed by a plateau lasting 2-3 ms. The relative brain motion reveals similar trend as the angular speed, and peaks near 20 ms. The average maximum principal strain reached its second peak near 17 ms during this increase in angular speed and relative displacement. As the angular speed decreases, the displacement begins to decreases as well, implying a return toward neutral for the brain. As the relative displacement crosses zero near 32 ms, a local minimum in the strain response occurs. As the relative brain motion then moves away its neutral position in the opposite direction, the strain response then begins to increase. At the time angular speed changes direction (43 ms), both the relative brain motion and the strain response reach their peaks. As the angular speed becomes more negative, the brain again tends towards neutral, accompanied by a simultaneous decrease in the strain responses. As the brain comes back again its neutral position near 62 ms, a local minimum occurs in the strain response.

Considering the two cases together, it seems that the strain magnitude increases as the brain moves away from its neutral position and decreases as the brain moves back to its neutral position. The strain may exhibit a local maximum as the relative displacement reaches its peak and a local minimum as the relative displacement crosses zero.

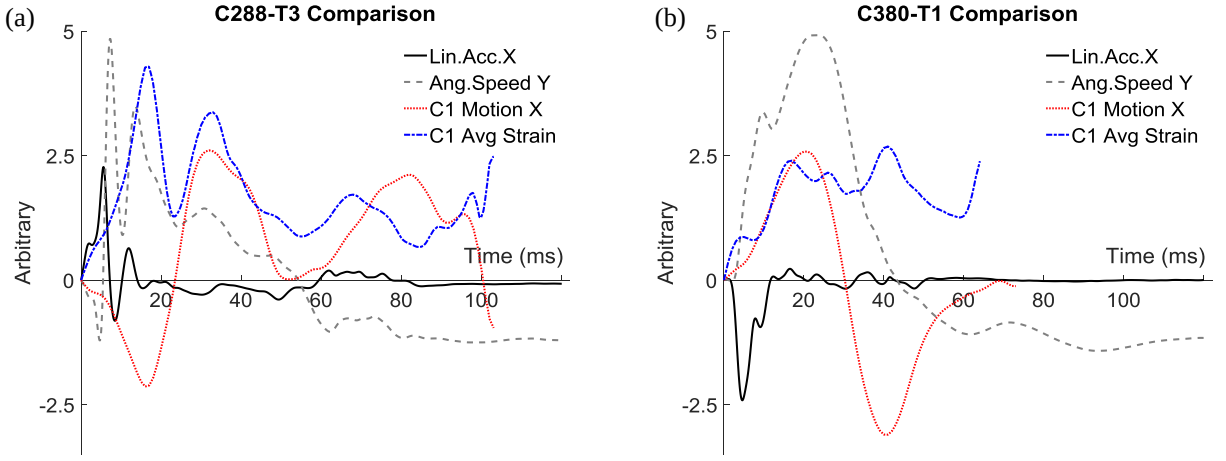

Figure 8. Comparison of kinematics trends for test C288-T3 (a) and C380-T1 (b). Parameters compared are linear acceleration, angular speed, C1 relative displacement, and revised average principal strain.

Consideration of FE head model validation

Greatest importance to FE modelling of the human head is the relevancy and accuracy of a model's validation. Although a universally accepted validation protocol for FE head models is still lacking, general consensus has been reached that it is not sufficient to validate FE head model for pressure and then predict response related to brain motion and deformation (Bradshaw and Morfey, 2001, Kleiven and Hardy, 2002, Zhao et al., 2015, Zhou et al., 2018). Agreement has not been reached regarding the suitability of using a model validated against brain-skull relative motion for brain deformation prediction. Under the same impact scenarios, models that have been validated against brain-skull relative displacement predict varying brain strain responses, resulting in significant disparity in brain injury prediction based on strain related metrics (Baeck, 2013, Giordano and Kleiven, 2016, Ji et al., 2014).

To better understand brain motion patterns, Zou et al. (2007) separated brain-skull relative motion data from Hardy et al. (2001) into a rigid-body component and a deformation component. The relative proportion of each component varied with impact severity: at low impact severity, the brain-skull relative motion was primarily dominated by the rigid-body component, while at higher impact severity, the deformation component contributed to most of the addition in brain-skull relative motion. This agrees with the insignificant correlations found in this study between the average cluster strain peaks and average cluster brain-skull relative motion peaks. However, it is important to note that, in both Hardy et al. (2001) and Hardy et al. (2007), most markers were not positioned to assess relative motion near the periphery, which would likely experience the majority of distortion in the brain during low-level impacts, resulting in the deeper brain having the appearance of rotating as a whole.

Considering the unique relationship between the brain-skull relative motion and its deformation component (Holzapfel, 2002, Zou et al., 2007), only under the condition that a brain model is "perfectly" validated against brain-skull relative motion, i.e. the model predicted exactly the same localized brain motion as the experimental data for all impact cases, could strain predictability of the given brain model be guaranteed. However, none of the existing FE head models has achieved such a "perfect" brain-skull relative motion validation result. Miller et al. (2016) evaluated the validation performance of several popular FE head models and found that the agreement in NDT displacement between experiment and simulation was reasonable for some cases and poor for others. Similar results are found in the current study. Given "imperfect" brain-skull relative motion validation, it is difficult to assert that a model validated by brain-skull relative motion could assure its brain strain prediction accuracy, which is solely depended on the deformation component of the brain-skull relative motion. This is supported also by the current findings, as no correlation was found between validation scores for brain-skull relative motion and brain strain. Thus, it is suggested that a brain model that might be used for strain prediction should validate its brain deformation against experimental brain strain data, e.g. the revised brain strain data from this study. Such a relevant comparison is expected to ensure confidence in the usage of FE head models for TBI prediction based on strain metrics.

As numerical surrogates of human head/brain, the FE models contain intrinsic insufficiencies in terms of geometrically and mechanically description of various anatomical structures as well as interaction representation between intracranial components. If the model is compared to an experimental parameter that is not the parameter of interest itself, it is suspected that numerical error might be introduced to the parameter of interest, especially in the condition that the parameter of interest is directly generated from the compared parameter via a chain of calculations (e.g. brain strain calculated from the brain-skull relative motion in the current study) with the propagation the inherent errors in the model. Thus, the intrinsic numerical deficiencies, which propagate and accumulate with the calculation process, further underscores the importance of a direct brain strain comparison between computationally obtained response and its experimentally determined counterpart.

In the current study, motion traces of the identified nodes representing NDTs are processed using multiple triads of targets to calculate the brain strain responses, which is the same as the NDT triad approach outlined by Hardy et al. (2007), except for the strain type presented. Details regarding the brain strain calculation approach were not presented in Chafi (2009) and Chafi et al. (2009). In Giordano and Kleiven (2014), a different approach was adopted in that the strain of the representing node was calculated for each NDT target and then averaged for all the nodes (referred as node average approach). As shown in Figure 9, when adopting the node average approach, neither the principal strain nor the shear strain is the same as those of NDT triad approach.

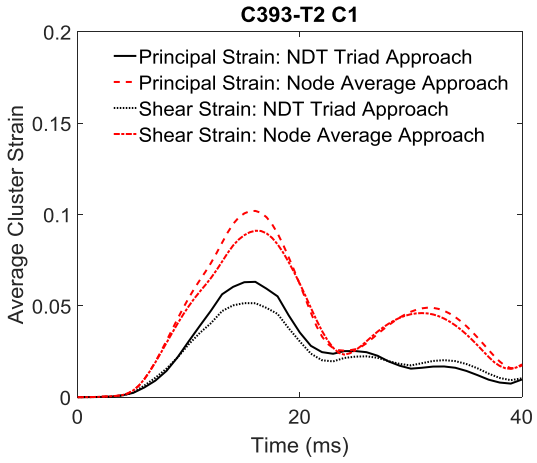

Figure 9. Comparison of brain strain calculation approaches from the current study and Giordano and Kleiven (2014).

A discussion regarding limitations is available in Hardy et al. (2007) for the experiments and in Kleiven and Hardy (2002) for the numerical simulations.

CONCLUSION

This study revisited the brain strain data from Hardy et al. (2007). The brain strain was recalculated by imposing the measured NDT motion to the NDT triad model. The revised brain strain data, along with the brain-skull relative motion data, were used to validate the KTH head model. Model validation performance was evaluated using both CORA and NISE. No significant correlations were noted, neither between the average cluster strain peaks and average cluster brain-skull relative motion peaks, nor between the computationally calculated brain strain validation scores and brain-skull relative motion validation scores. This lack of correlation indicates that validating a model against brain-skull relative motion might be insufficient to assure the strain prediction accuracy of the given model. Therefore, it is suggested that a model intended to be used for strain prediction should be validated against experimental brain deformation data, e.g. the revised brain strain data from this study, in addition to brain-skull relative motion.

ACKNOWLEDGMENTS

This research has received funding from the European Union's Horizon 2020 research and innovation program under the Marie-Curie grant agreement No. 642662. The authors declare that they have no conflict of interest.

REFERENCES

Adams, J., Graham, D., and Gennarelli, T. (1981) Acceleration induced head injury in the monkey. II. Neuropathology. In Experimental and Clinical Neuropathology, pp. 26-28. Springer.

Al-Bsharat, A.S., Hardy, W.N., Yang, K.H., Khalil, T.B., Tashman, S., and King, A.I. (1999) Brain/skull relative displacement magnitude due to blunt head impact: new experimental data and model. Proc. 43rd Stapp Car Crash Conference, pp. 321-332. Society of Automative Engineers, Warrendale, PA.

Alshareef, A., Giudice, J.S., Forman, J., Salzar, R.S., and Panzer, M.B. (2017) A Novel Method for Quantifying Human In Situ Whole Brain Deformation Under Rotational Loading Using Sonomicrometry. Journal of Neurotrauma 35 (5): 780-789.

Baeck, K. (2013) Biomechanical Modeling of Head Impacts–A Critical Analysis of Finite Element Modeling Approaches. Ph.D. Dissertation, KU Leuven

Bayly, P., Cohen, T., Leister, E., Ajo, D., Leuthardt, E., and Genin, G. (2005) Deformation of the human brain induced by mild acceleration. Journal of Neurotrauma 22 (8): 845-856.

Bradshaw, D., and Morfey, C. (2001) Pressure and shear response in brain injury models. Proc. 17th International Technical Conference on the Enhanced Safety of Vehicles. National Highway Traffic Safety Administration, Amsterdam, The Netherlands.

Chafi, M.S. (2009) Biomechanical analysis of blast-induced traumatic brain injury using multiscale brain modeling. Ph.D. Dissertation, North Dakota State University.

Chafi, M.S., Dirisala, V., Karami, G., and Ziejewski, M. (2009) A finite element method parametric study of the dynamic response of the human brain with different cerebrospinal fluid constitutive properties. Proceedings of the Institution of Mechanical Engineers, Part H: Journal of Engineering in Medicine 223 (8): 1003-1019.

Chason, J., Hardy, W., Webster, J., and Gurdjian, E. (1958) Alterations in cell structure of the brain associated with experimental concussion. Journal of Neurosurgery 15 (2): 135-139.

DiMasi, F.P., Eppinger, R.H., and Bandak, F.A. (1995) Computational analysis of head impact response under car crash loadings. Proc. 39th Stapp Car Crash Conference, pp. 425-438. Society of Automative Engineers, Warrendale, PA.

Donnelly, B.R., Morgan, R.M., and Eppinger, R.H. Durability, repeatability and reproducibility of the NHTSA side impact dummy. Proc. 27th Stapp Car Crash Conference, pp. 299-310. Society of Automotive Engineers, San Diego, CA.

Drake, A.M., Takhounts, E.G., and Hasija, V. (2017) Investigation of parameters affecting brain model validation and brain strains using the SIMon finite element head model. Proc. IRCOBI Conference, pp. 410-431. Antwerp, Belgium.

Feng, Y., Abney, T.M., Okamoto, R.J., Pless, R.B., Genin, G.M., and Bayly, P.V. (2010) Relative brain displacement and deformation during constrained mild frontal head impact. Journal of The Royal Society Interface 7 (53): 1677-1688.

Gehre, C., Gades, H., and Wernicke, P. Objective rating of signals using test and simulation responses. Proc. 21st International Technical Conference on the Enhanced Safety of Vehicles. National Highway Traffic Safety Administration, Stuttgart, Germany.

Gennarelli, T., Adams, J., and Graham, D. (1981) Acceleration induced head injury in the monkey. I. The model, its mechanical and physiological correlates. In Experimental and Clinical Neuropathology, pp. 23-25. Springer.

Gennarelli, T.A., Thibault, L.E., Adams, J.H., Graham, D.I., Thompson, C.J., and Marcincin, R.P. (1982) Diffuse axonal injury and traumatic coma in the primate. Annals of Neurology 12 (6): 564-574.

Giordano, C., Cloots, R., Van Dommelen, J., and Kleiven, S. (2014) The influence of anisotropy on brain injury prediction. Journal of Biomechanics 47 (5): 1052-1059.

Giordano, C., and Kleiven, S. (2014) Evaluation of axonal strain as a predictor for mild traumatic brain injuries using finite element modeling. Stapp Car Crash Journal 58: 29-61.

Giordano, C., and Kleiven, S. (2016) Development of an unbiased validation protocol to assess the biofidelity of finite element head models used in prediction of traumatic brain injury. Stapp Car Crash Journal 60: 363-471.

Guettler, A., Ramachandra, R., Bolte, J., and Hardy, W. (2018) Kinematics Response of the PMHS Brain to Rotational Loading of the Head: Development of Experimental Methods and Analysis of Preliminary Data. SAE Technical Paper: 2018-01-0547.

Gurdjian, E.S., Lissner, H., Evans, F., Patrick, L., and Hardy, W. (1961) Intracranial pressure and acceleration accompanying head impacts in human cadavers. Surgery, Gynecology and Obstetrics 113: 185-190.

Hardy, W.N. (2002) Instrumentation in experimental design. In Accidental Injury, pp. 12-39. Springer.

Hardy, W.N. (2007) Response of the human cadaver head to impact. Ph.D. Dissertation, Wayne State University.

Hardy, W.N., Foster, C.D., Mason, M.J., Yang, K.H., King, A.I., and Tashman, S. (2001) Investigation of head injury mechanisms using neutral density technology and high-speed biplanar X-ray. Stapp Car Crash Journal 45: 337-368.

Hardy, W.N., Khalil, T.B., and King, A.I. (1994) Literature review of head injury biomechanics. International Journal of Impact Engineering 15 (4): 561-586.

Hardy, W.N., Mason, M.J., Foster, C.D., Shah, C.S., Kopacz, J.M., Yang, K.H., King, A.I., Bishop, J., Bey, M., and Anderst, W. (2007) A study of the response of the human cadaver head to impact. Stapp Car Crash Journal 51: 17.

Ho, J., Zhou, Z., Li, X., and Kleiven, S. (2017) The peculiar properties of the falx and tentorium in brain injury biomechanics. Journal of Biomechanics 60: 243-247.

Holbourn, A. (1943) Mechanics of head injuries. The Lancet 242 (6267): 438-441.

Holzapfel, G.A. (2002) Nonlinear solid mechanics: a continuum approach for engineering science. Chichester: Wiley.

Horgan, T.J., and Gilchrist, M.D. (2003) The creation of three-dimensional finite element models for simulating head impact biomechanics. International Journal of Crashworthiness 8 (4): 353-366.

Iwamoto, M., and Nakahira, Y. (2015) Development and Validation of the Total HUman Model for Safety (THUMS) Version 5 Containing Multiple 1D Muscles for Estimating Occupant Motions with Muscle Activation During Side Impacts. Stapp Car Crash Journal 59: 53-90.

Ji, S., Ghadyani, H., Bolander, R.P., Beckwith, J.G., Ford, J.C., McAllister, T.W., Flashman, L.A., Paulsen, K.D., Ernstrom, K., and Jain, S. (2014) Parametric comparisons of intracranial mechanical responses from three validated finite element models of the human head. Annals of Biomedical Engineering 42 (1): 11-24.

Ji, S., Zhu, Q., Dougherty, L., and Margulies, S.S. (2004) In vivo measurements of human brain displacement. Stapp Car Crash Journal 48: 227-237.

King, A.I., Yang, K.H., Zhang, L., Hardy, W., and Viano, D.C. Is head injury caused by linear or angular acceleration. Proc. IRCOBI Conference, pp. 1-12. Lisbon, Portugal.

Kleiven, S. (2002) Finite element modeling of the human head. Ph.D. Dissertation, Kungliga Tekniska Högskolan.

Kleiven, S. (2006) Evaluation of head injury criteria using a finite element model validated against experiments on localized brain motion, intracerebral acceleration, and intracranial pressure. International Journal of Crashworthiness 11 (1): 65-79.

Kleiven, S. (2007) Predictors for traumatic brain injuries evaluated through accident

reconstructions. Stapp Car Crash Journal 51: 81-114.

Kleiven, S. (2013) Why most traumatic brain injuries are not caused by linear acceleration but skull fractures are. Frontiers in Bioengineering and Biotechnology 1: 1-5.

Kleiven, S., and Hardy, W.N. (2002) Correlation of an FE model of the human head with local brain motion: Consequences for injury prediction. Stapp Car Crash Journal 46: 123-144.

Knutsen, A.K., Magrath, E., McEntee, J.E., Xing, F., Prince, J.L., Bayly, P.V., Butman, J.A., and Pham, D.L. (2014) Improved measurement of brain deformation during mild head acceleration using a novel tagged MRI sequence. Journal of Biomechanics 47 (14): 3475-3481.

Mao, H., Zhang, L., Jiang, B., Genthikatti, V.V., Jin, X., Zhu, F., Makwana, R., Gill, A., Jandir, G., and Singh, A. (2013) Development of a finite element human head model partially validated with thirty five experimental cases. Journal of Biomechanical Engineering 135 (11): 357-366.

Margulies, S.S., Thibault, L.E., and Gennarelli, T.A. (1990) Physical model simulations of brain injury in the primate. Journal of Biomechanics 23 (8): 823-836.

Masuzawa, H., Nadamura, N., Hirakawa, K., Sano, K., and Matsuno, M. (1976) Experimental head injury & concussion in monkey using pure linear acceleration impact. Neurologia medico-chirurgica (Tokyo) 16 (PT1): 77-90.

Mayberry, T. (2008) Analysis and Modeling of Relative Brain Motion for Various Head Impact Scenarios. Master Thesis, The Ohio State University.

Meaney, D., Smith, D., Shreiber, D., Bain, A., Miller, R., Ross, D., and Gennarelli, T. (1995) Biomechanical analysis of experimental diffuse axonal injury. Journal of Neurotrauma 12 (4): 689-694.

Miller, L.E., Urban, J.E., and Stitzel, J.D. (2016) Development and validation of an atlas-based finite element brain model. Biomechanics and Modeling in Mechanobiology 15 (5): 1201-1214.

Nahum, A.M., Smith, R., and Ward, C.C. Intracranial pressure dynamics during head impact. Proc. 21st Stapp Car Crash Conference, pp. 337-366. Society of Automotive Engineers, Warrendale, PA.

Nusholtz, G.S., Lux, P., Kaiker, P., and Janicki, M.A. Head impact response—Skull deformation and angular accelerations. Proc. 28th Stapp Car Crash Conference, pp. 41-74. Warrendale, PA.

Ommaya, A., and Hirsch, A. (1971) Tolerances for cerebral concussion from head impact and whiplash in primates. Journal of Biomechanics 4 (1): 13-21.

Sabet, A.A., Christoforou, E., Zatlin, B., Genin, G.M., and Bayly, P.V. (2008) Deformation of the human brain induced by mild angular head acceleration. Journal of Biomechanics 41 (2): 307-315.

Stalnaker, R., Melvin, J., Nusholtz, G., Alem, N., and Benson, J. Head impact response. Proc. 21st Stapp Car Crash Conference, pp. 303-335. Society of Automotive Engineers, Warrendale, PA.

Takhounts, E.G., Craig, M.J., Moorhouse, K., McFadden, J., and Hasija, V. (2013) Development of Brain Injury Criteria (BrIC). Stapp Car Crash Journal 57: 243-266.

Takhounts, E.G., Ridella, S.A., Hasija, V., Tannous, R.E., Campbell, J.Q., Malone, D., Danelson, K., Stitzel, J., Rowson, S., and Duma, S. (2008) Investigation of traumatic brain injuries using the next generation of simulated injury monitor (SIMon) finite element head model. Stapp Car Crash Journal 52: 1-31.

Trosseille, X., Tarriere, C., Lavaste, F., Guillon, F., and Domont, A. Development of a FEM of the human head according to a specific test protocol. Proc. Proc. 28th Stapp Car Crash Conference, pp. 235-253. Society of Automotive Engineers, Warrendale, PA.

Unterharnscheidt, F., and Higgins, L.S. (1969) Pathomorphology of experimental head injury due to rotational acceleration. Acta Neuropathologica 12 (2): 200-204.

VandeVord, P.J., Leung, L.Y., Hardy, W., Mason, M., Yang, K.H., and King, A.I. (2008) Up-regulation of reactivity and survival genes in astrocytes after exposure to short duration overpressure. Neuroscience Letters 434 (3): 247-252.

Viano, D.C., Casson, I.R., Pellman, E.J., Zhang, L., King, A.I., and Yang, K.H. (2005) Concussion in professional football: brain responses by finite element analysis: part 9. Neurosurgery 57 (5): 891-916.

von Holst, H., and Li, X. (2013) Consequences of the dynamic triple peak impact factor in traumatic brain injury as measured with numerical simulation. Frontiers in Neurology 4: 23.

Zhao, W., Cai, Y., Li, Z., and Ji, S. (2017) Injury prediction and vulnerability assessment using strain and susceptibility measures of the deep white matter. Biomechanics and Modeling in Mechanobiology 16 (5): 1709-1727.

Zhao, W., Ruan, S., and Ji, S. (2015) Brain pressure responses in translational head impact: a dimensional analysis and a further computational study. Biomechanics and Modeling in Mechanobiology 14 (4): 753-766.

Zhou, Z., Li, X., and Kleiven, S. (2018) Fluid–structure interaction simulation of the brain–skull interface for acute subdural haematoma prediction. Biomechanics and Modeling in Mechanobiology: 1-19.

Zou, H., Kleiven, S., and Schmiedeler, J.P. (2007) The effect of brain mass and moment of inertia on relative brain–skull displacement during low-severity impacts. International Journal of Crashworthiness 12 (4): 341-353.

Zou, H., Schmiedeler, J.P., and Hardy, W.N. (2007) Separating brain motion into rigid body displacement and deformation under low-severity impacts. Journal of Biomechanics 40 (6): 1183-1191.

APPENDIX A: EXPERIMENTAL BRAIN STRAIN FOR CLUSER 2 IN C380

Considering the scarcity of the coronal and horizontal impacts in Hardy et al. (2007) and the consistency of the suspected NDT traces, i.e. traces of NDT 9, in cluster 2 (C2) for the six impacts delivered to C380, an exceptional triad model is developed to derive the strain of C2 based on the remaining six NDTs with reliable traces. Representative FE nodes were generated based on the NDT starting position. Each node was connected to its neighboring nodes to form 8 triads (Figure A1). Maximum principal strain and shear strain are obtained from the simulation by imposing the tracked NDT motion in experiments relative to the skull on this specific triad model. The results from the eight triad elements are averaged for each NDT cluster and plotted in Figure A2.

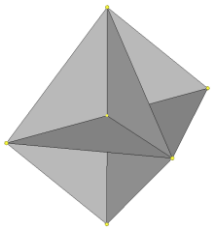

Figure A1. The exceptional triad model used for strain calculation for C2 in C380.

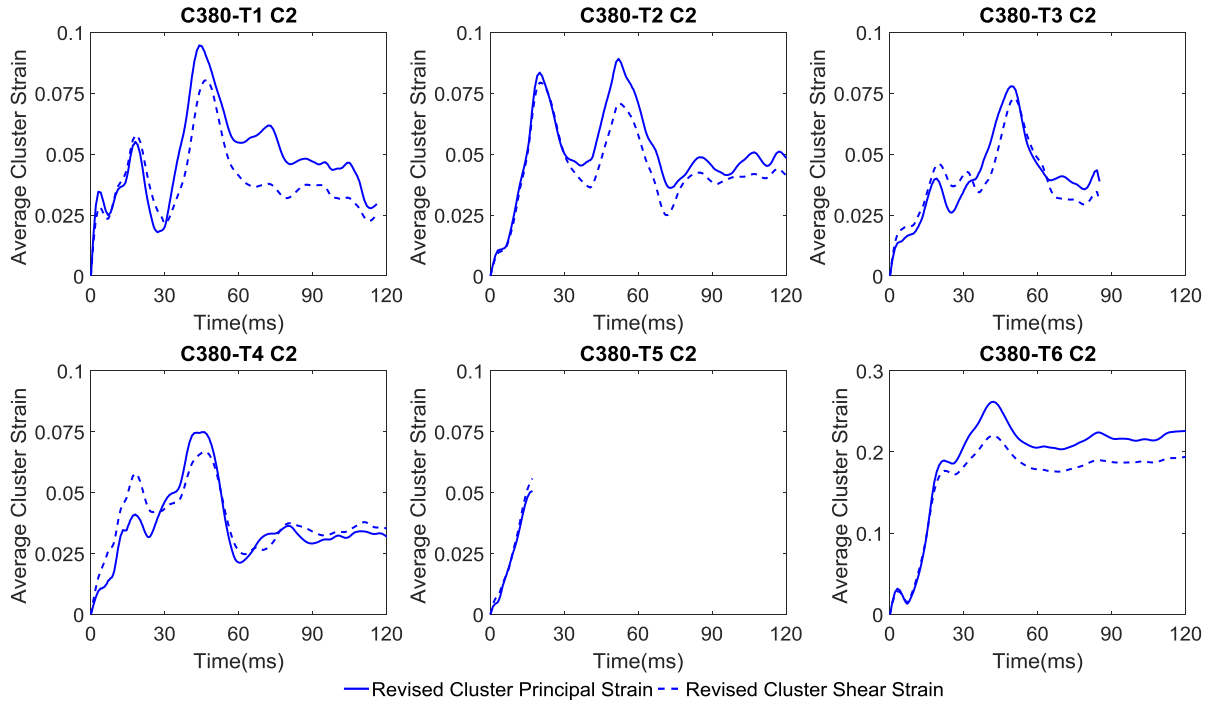

Figure A2. Strain response of C2 in C380.

APPENDIX B: VALIDATION RESULTS OF BRAIN-SKULL RELATIVE MOTION

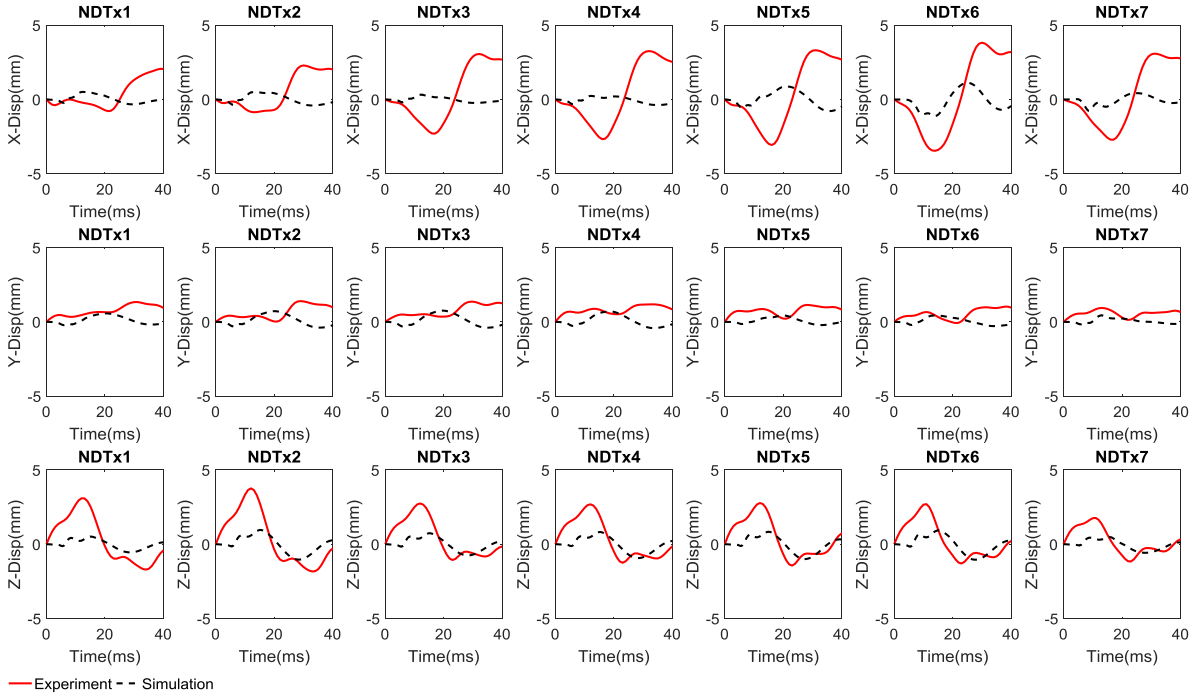

Figure B1. Comparison between experimental data and simulated brain-skull relative displacement for the experiment C288-T3 C1.

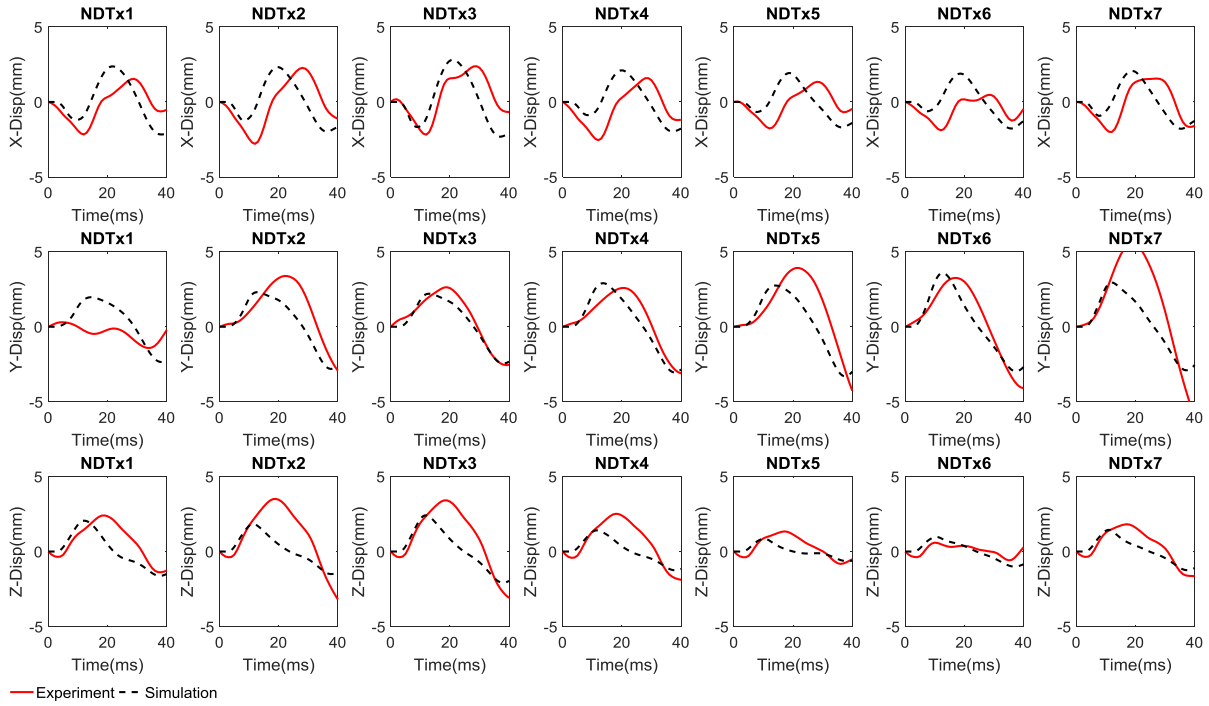

Figure B2. Comparison between experimental data and simulated brain-skull relative displacement for the experiment C380-T1 C1.

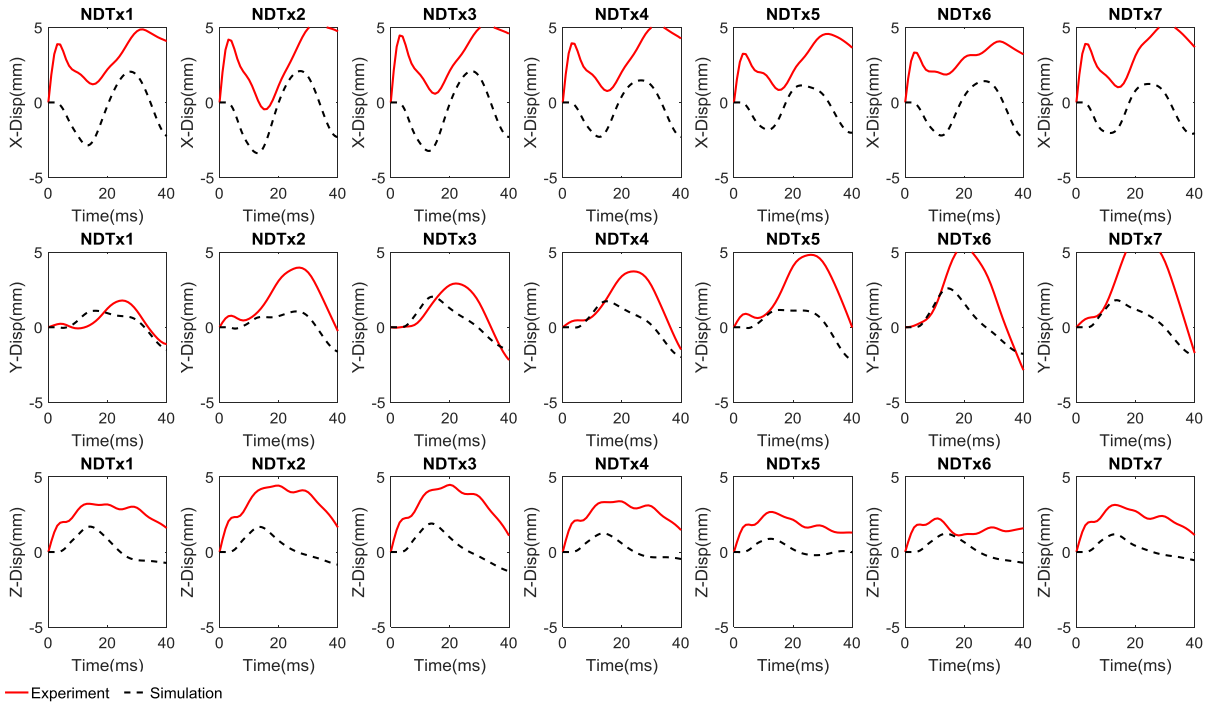

Figure B3. Comparison between experimental data and simulated brain-skull relative displacement for the experiment C380-T2 C1.

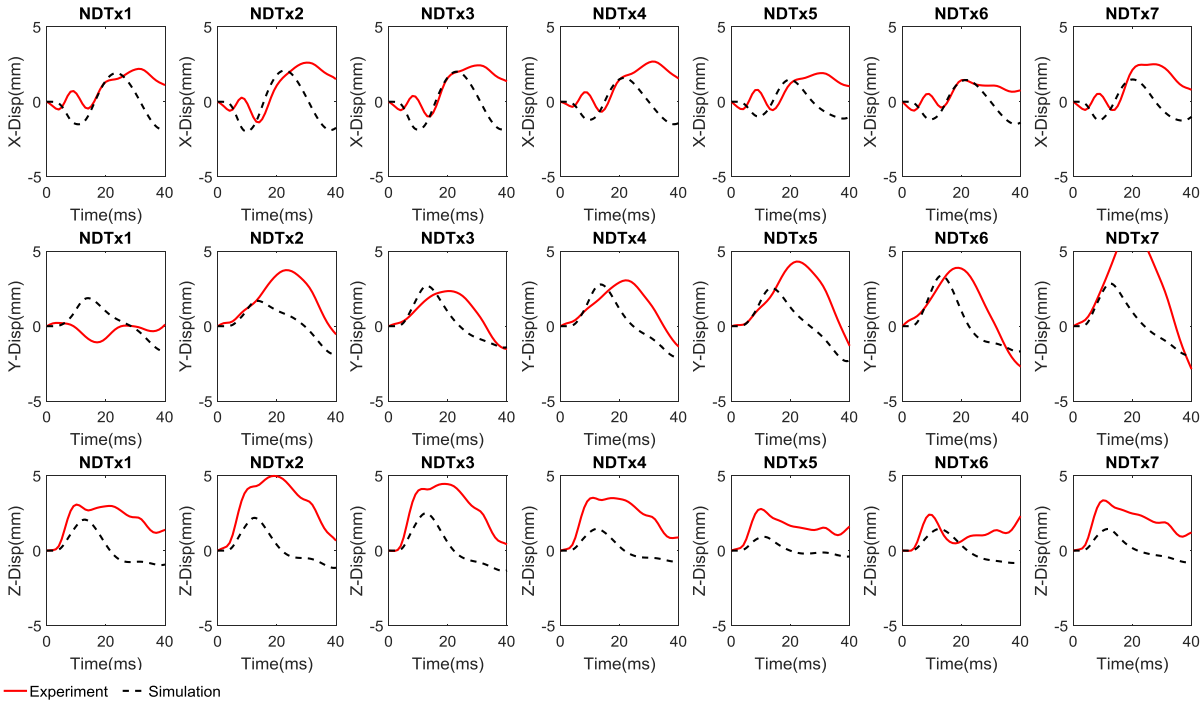

Figure B4. Comparison between experimental data and simulated brain-skull relative displacement for the experiment C380-T3 C1.

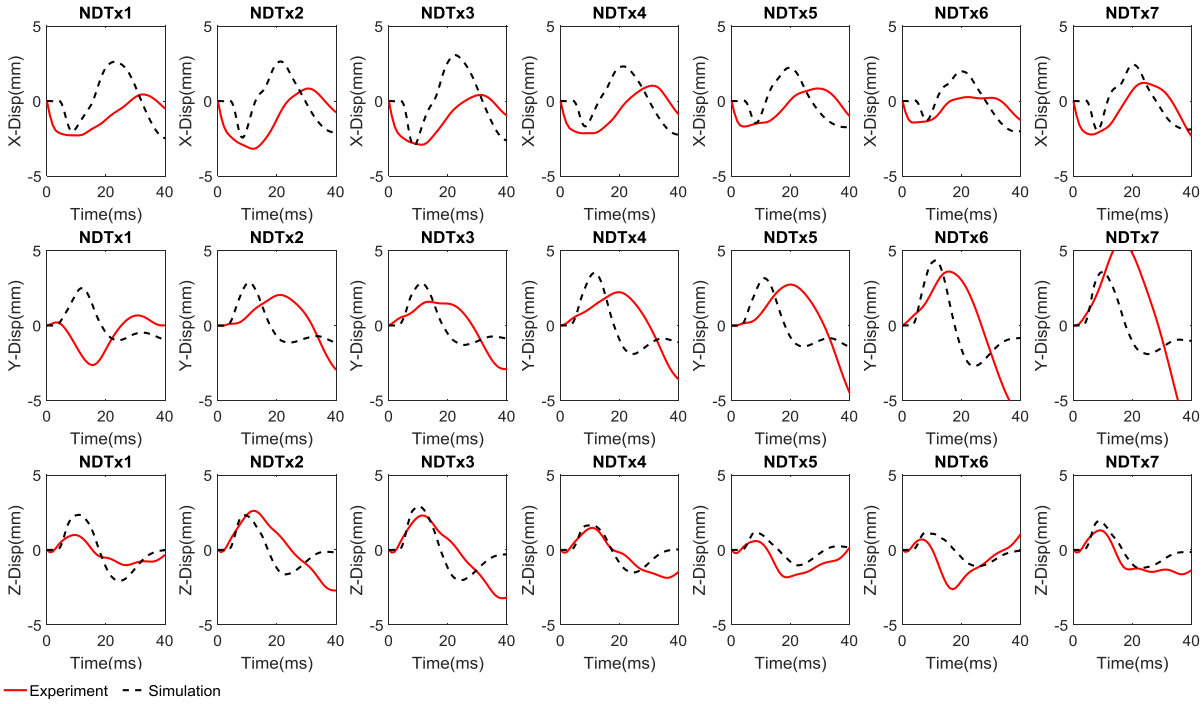

Figure B5. Comparison between experimental data and simulated brain-skull relative displacement for the experiment C380-T4 C1.

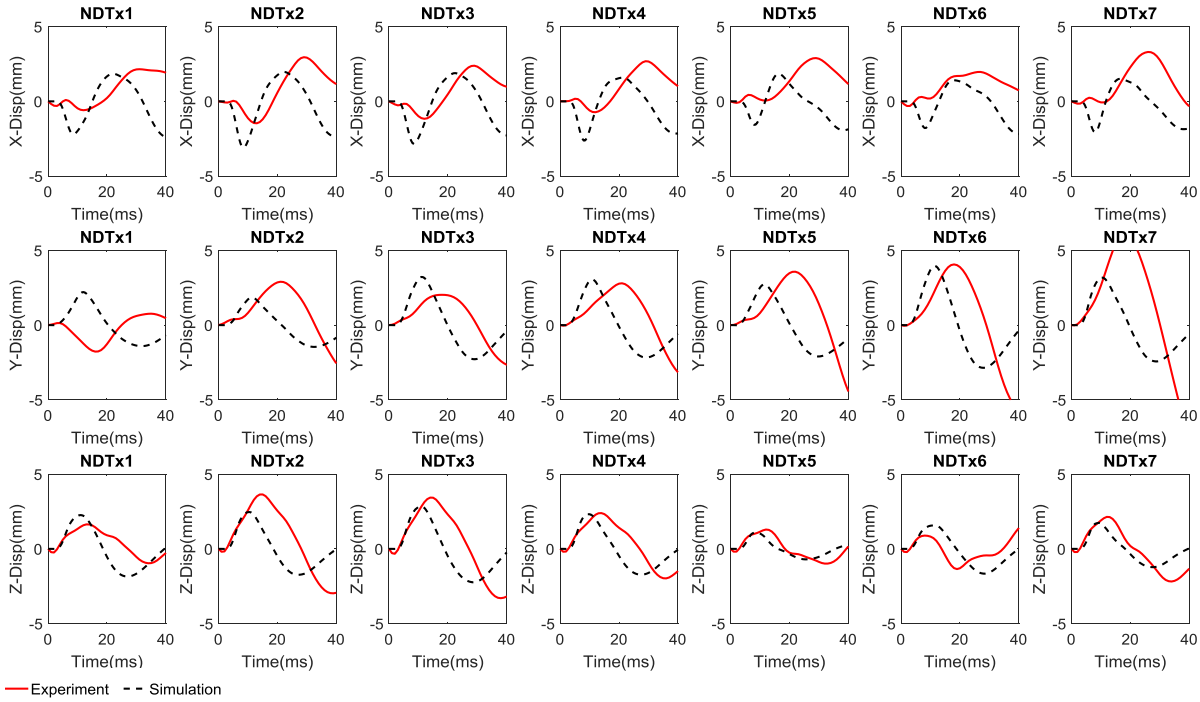

Figure B6. Comparison between experimental data and simulated brain-skull relative displacement for the experiment C380-T6 C1.

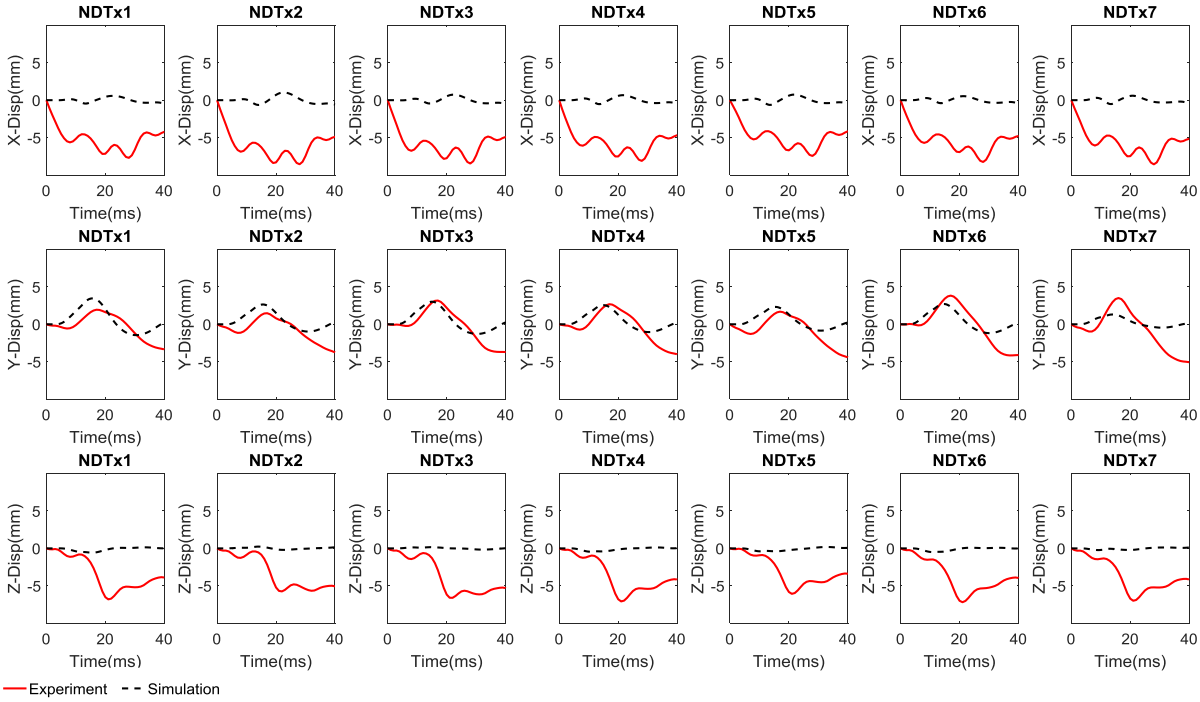

Figure B7. Comparison between experimental data and simulated brain-skull relative displacement for the experiment C393-T2 C1.

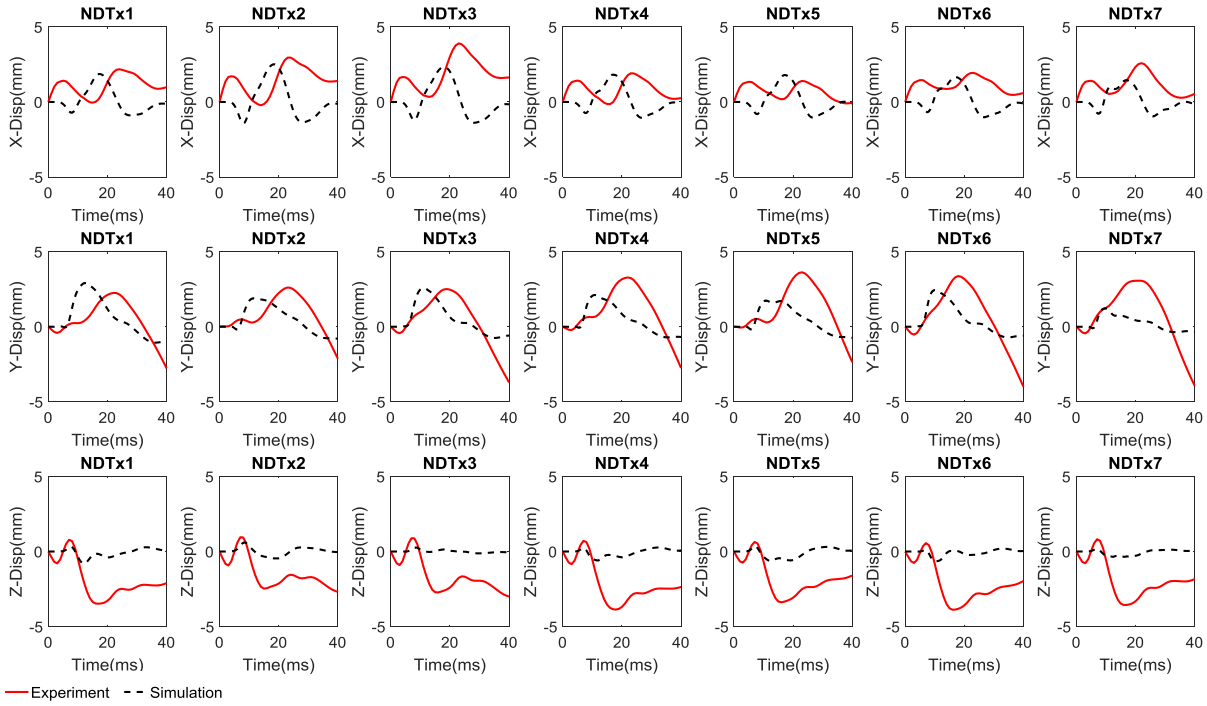

Figure B8. Comparison between experimental data and simulated brain-skull relative displacement for the experiment C393-T3 C1.